Structures on electron temperature profiles in the RTP plasma

Steenbakkers, M.F.M.

Award date:
1995

FOM-instituut voor
Plasmafysica
"Rijnhuizen"
Nieuwegein

IR 95/???
June 1995

Structures on electron temperature profiles in the RTP plasma

M.F.M. Steenbakkers

FOM-instituut voor Plasmafysica "Rijnhuizen", Association Euratom-FOM
P.O. Box 1207, 3430 BE Nieuwegein

FOM-instituut voor
Plasmafysica
"Rijnhuizen"
Nieuwegein

IR 95/???
June 1995

Structures on electron temperature profiles in the RTP plasma

M.F.M. Steenbakkers

Acknowledgement

This report describes the work that I have carried out to obtain my degree at the Technical University of Eindhoven. The research was done under supervision of Prof. Dr. N.J. Lopes Cardozo, Dr. C.C. Chu and Dr. ir. F.J. Pijper in the RTP group of FOM-instituut voor Plasmafysica "Rijnhuizen". This work was carried out at FOM-instituut voor Plasmafysica "Rijnhuizen" under the Euratom-FOM association agreement, with financial support from NWO and Euratom.

Abstract

It is often assumed that the magnetic topology in a tokamak is formed by a nest of toroidal flux surfaces. High resolution measurements of electron temperature and density with multiposition Thomson scattering in the RTP tokamak indicate that the magnetic topology is more complex. In plasmas heated with central electron cyclotron heating, high peaks (filaments) are observed in the center of the plasma, steep gradients near the sawtooth inversion radius and structures outside the sawtooth inversion region. In resistively heated plasmas structures are observed both inside and outside the sawtooth inversion region. Measurements done with a changed Thomson scattering set-up showed a decrease of the height of the filaments. To be sure that the measured structures are not an artefact of the Thomson scattering measuring technique, the measured electron temperature profiles have been statistically analyzed by the use of two methods:

- Power spectral analysis (Fourier analysis).
- Free knot cubic spline fitting. The profiles are fitted with a cubic spline with an increasing number of knots. The best fit is selected with the F-test.

The methods have been tested by applying them to simulated measurements of electron temperature profiles. From the statistical analysis it follows that observed structures are significant down to 1 cm. Furthermore it is shown that the decrease in the height of the filaments is not caused by the change in Thomson scattering set-up.

Contents

Chapter 1

Introduction

As natural resources for conventional energy production are running out, much research is done on alternative ways of producing energy. A good candidate is thermonuclear fusion, since fusion fuel is abundantly available and the products of the fusion reaction are not radioactive. Most research in this field is done on so called tokamaks: in these fusion reactors the thermonuclear plasma is confined in a torus shaped configuration by a helical magnetic field, consisting of a toroidal field created by external coils and a poloidal field generated by the toroidal plasma current. It is often assumed that this field forms a nest of closed flux surfaces. Because currents and magnetic field lines lie in these magnetic surfaces the gradients of electron and ion pressure (p_e and p_i) are perpendicular to these surfaces, according to $\vec{j} \times \vec{B} = \nabla p$. This assumption implies that p_e, electron temperature (T_e) and electron density (n_e) profiles are smooth and, in the absence of central sinks, monotonic functions of the radius. The fact that energy losses in the plasma are unexpectedly high has given rise to doubts about the assumption of closed magnetic surfaces. Measurements done at severals tokamaks give support to these doubts. At the Rijnhuizen Tokamak Project (RTP) measurements of p_e, T_e and n_e with the multiposition Thomson Scattering (TS) diagnostic give indications that the magnetic topology is more complex and may be represented by small scale filamented structures surrounded by regions of stochastic field [Lop94]. Figure 1.1 gives an impression of the magnetic topology. Figure 1.2 compares a p_e profile of the type expected on the basis of the theory of closed flux surfaces with a p_e profile measured in RTP. The measured profile shows structures and high peaks with steep gradients indicating regions of low energy transport.

The question arises: Are the structures really caused by plasma effects or by the way they are measured? There are several ways to give an answer to this question. In this report we have chosen to test the significance of the structures in a statistical way. The statistical analysis of the structures requires detailed knowledge of the statistical and systematical errors of the measurement. For this reason extended simulations have been carried out [Chu94]. The statistical analysis has been applied to different series of plasma discharges of similar plasma conditions (Ohmic or resistively heated plasmas and plasmas heated by electron cyclotron heating (ECH) for two different set-ups).
Two statistical methods have been used:

- Power Spectrum (PS) analysis.
- Free Knot Cubic Spline Fitting (FK), a way to find the best fit through the profiles.

Beforehand the methods have been 'calibrated' by applying them to simulated measurements of smooth T_e profiles with noise added.

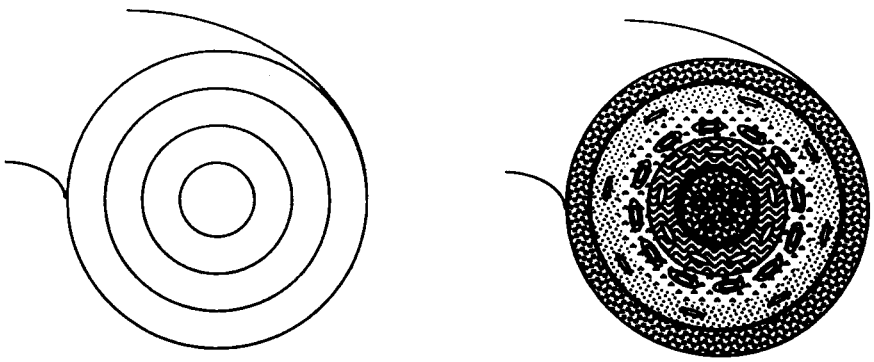

Figure 1.1: *On the left the simple magnetic topology: a nest of closed flux surfaces. On the r*
a complex topology: filamentary structures surrounded by regions of stochastic field.

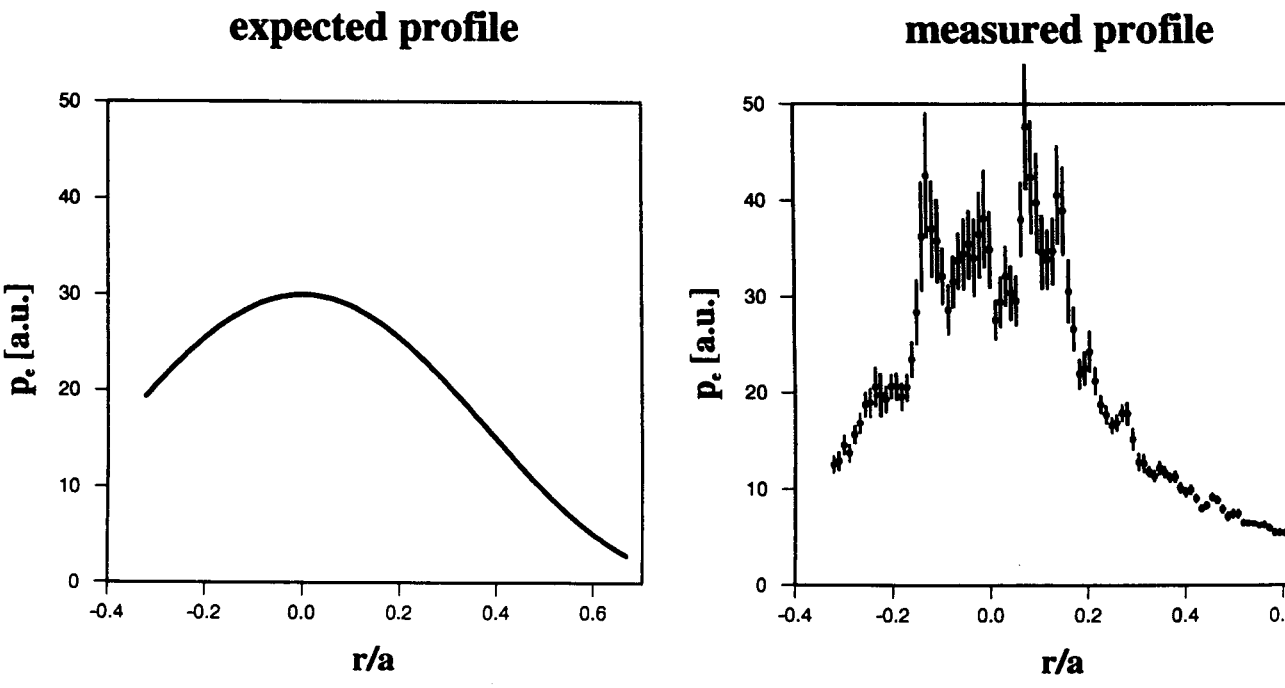

Figure 1.2: p_e *as predicted by the theory of closed flux surfaces (left) and a measured* p_e *pro*

Chapter 2

Experiment

2.1 Tokamak

For nuclear fusion to take place the nuclei should be within the range of their strong interactions. The Coulomb force prevents this from happening for plasmas at low temperatures. The cross section for the most promising reaction

$$D + T \longrightarrow {}^{4}_{2}He + n + 17.58 \text{ MeV} \tag{2.1}$$

reaches its maximum for particle energies of 100 keV. For tokamaks a temperature of about 10 keV i.e. approximately 10^8 K should be enough, as the particles in the tail of the velocity distribution have sufficiently high energies to produce a reasonable number of reactions. At such temperatures the fuel is fully ionized (plasma).

Clearly the plasma should not make contact with the walls. This can be achieved by confining the plasma in a magnetic field. In equilibrium the net pressure outwards is compensated by the Lorentz force

$$\vec{j} \times \vec{B} = \nabla p. \tag{2.2}$$

The hitherto most successful way to come close to the conditions for breakeven has been with the tokamak configuration, which is pictured schematically in Fig. 2.1. The basic components of the tokamak are:

- a vacuum vessel in the shape of a torus, in which the plasma is maintained.
- coils to produce a toroidal magnetic field.
- coils serving as the primary winding of a transformer. The secondary winding is formed by the plasma itself. In this way a toroidal current is created with a twofold purpose:
  - resistive heating of the plasma.
  - generation of a poloidal magnetic field, which is necessary to prevent the plasma from drifting outwards.
- a transformer yoke, to couple the magnetic flux swing produced by the primary winding to the secondary winding, i.e. the plasma.
- coils producing horizontal and vertical fields to control the position of the plasma.

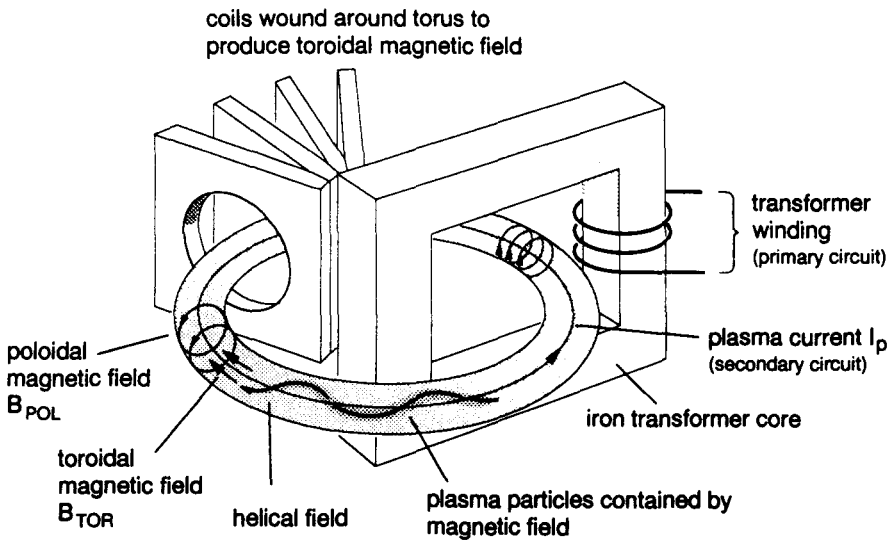

Figure 2.1: *A schematic view of a tokamak.*

- additional heating systems such as neutral beam injection and RF heating. ECH is a fo of RF heating.
- systems for vessel conditioning and vacuum conditioning.

To observe the features of the plasma a number of diagnostic systems is attached to the tokam The current driven through the plasma is limited in time and therefore plasmas can only created in a pulsed form. The pulses vary from hundreds of milliseconds in small tokamaks minutes in the bigger ones. To get statistically enough measurements plasma discharges w the same conditions may have to be repeated several times.

2.2 RTP

The measurements were performed in the Rijnhuizen tokamak RTP (major radius = 0.72 minor radius = 0.164 m, plasma current = 40 – 150 kA, toroidal magnetic field < 2.35 T) which the research program is dedicated to transport phenomena in tokamak plasmas. In addi to ohmic heating the plasma can be heated by means of ECH, for which three gyrotrons h been installed: a 60 GHz gyrotron applied from the low field side (60 – 180 kW, pulse dura 100 ms), a 60 GHz gyrotron on the high field side (180 kW, 100 ms) and a 110 GHz gyro (500 kW, 200 ms) on the low field side. Thanks to the (in comparison to other tokamaks) g access to the tokamak many diagnostics could be installed:

- magnetics, to measure the magnetic field, the plasma current, the plasma position and shape of the plasma
- a 2 mm interferometer measuring the line integrated electron density along a chord thro the center of the plasma
- a Michelson interferometer for ECE

- a multiposition Thomson scattering diagnostic measuring T_e and n_e
- a 20 channel heterodyne electron radiometer measuring electron cyclotron emission (ECE) and electron cyclotron absorption (ECA)
- a 19 channel far infrared interferometer/polarimeter measuring the line averaged electron density and the Faraday rotation angle
- a 80 channel 5 camera soft x-ray tomographic system
- a 80 channel 5 camera visible light tomographic system
- a pulsed radar system to measure n_e profiles
- visible light, VUV and XUV spectroscopic systems
- a diagnostic measuring the transmitted ECH power
- a bolometer measuring the radiation loss from the plasma.

To study transport the plasma can be perturbed by repeatedly switching on and off ECH and by injecting pellets of frozen hydrogen. The installed pellet injector can inject 8 pellets per discharge at velocities of 0.4 – 1 km/s. The pellets consist of $5 - 20 \cdot 10^{18}$ particles, which is about as much as the number of particles already in the torus: for a line averaged density of $2.5 \cdot 10^{19} m^{-3}$ the number of ions in the plasma is $1 \cdot 10^{19}$.

2.3 Thomson scattering

2.3.1 Principle of Thomson scattering

Thomson scattering is the scattering of electromagnetic radiation on free electrons in the pla
Under certain circumstances the electrons radiate under influence of the electric field of
incoming electromagnetic wave like dipole radiators. In Fig. 2.2 the geometry of the scatte
process is shown [1]. The incoming wave has frequency ω_0 and wave vector $\vec{k}_0$, whereas

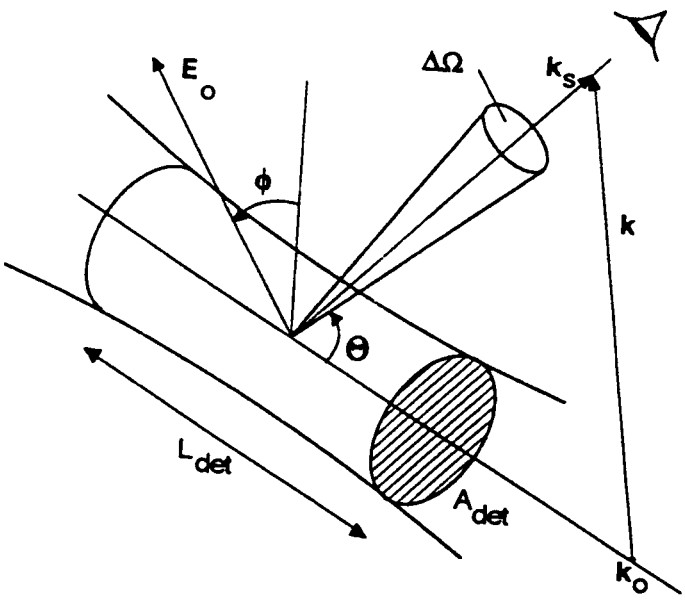

Figure 2.2: *The scattering geometry.*

scattered wave has frequency ω_s and wave vector $\vec{k}_s$. The polarization angle is denoted b
the scattering angle by θ. The detection volume is $V_{det} = A_{det} \times L_{det}$. The scattering vector
given by

$$\vec{k} = \vec{k}_s - \vec{k}_0. \quad ($$

The frequency of the scattered wave has a Doppler shift ω with respect to the frequency of
incoming wave

$$\omega = \omega_s - \omega_0 = \vec{k} \cdot \vec{v}, \quad ($$

with $\vec{v}$ the velocity of the electron. The scattering on more than one electron can be character
by the scattering parameter α

$$\alpha = \frac{1}{k\lambda_D}, \quad ($$

with the Debye length $\lambda_D = \sqrt{\frac{\epsilon_0 k_B T_e}{e^2 n_e}}$, i.e. the shielding distance for electric fields in a plasm
If $\alpha \ll 1$, the process is referred to as incoherent TS. In this case the incident has a wavelen
much smaller than λ_D and 'sees' the individual electrons.

[1] This figure was taken from [San91]

If $\alpha > 1$, the process is referred to as coherent TS. Now the wave is scattered on groups of charges, which is called collective scattering. In the considered RTP plasmas α is smaller than 0.01, which places our TS experiments in the incoherent TS regime. The power scattered in the frequency range $d\omega_s$ and in the solid angle $\Delta\Omega$ is given by [San91] [She75]

$$P_s(\vec{k},\omega)\, d\omega_s = P_0\, n_e\, L_{det}\, \Delta\Omega\, g(\theta,\phi)\, S(\vec{k},\omega)\, \frac{d\sigma_T}{d\Omega}\, d\omega_s, \tag{2.6}$$

where P_s and P_0 are the scattered and incident power respectively. The differential cross section for TS $\frac{d\sigma_T}{d\Omega}$ equals ${r_e}^2$

$$\frac{d\sigma_T}{d\Omega} = {r_e}^2 = \left(\frac{e^2}{4\pi\epsilon_0 m_e c^2}\right)^2 = 7.94 \cdot 10^{-30} m^2, \tag{2.7}$$

where r_e is the classical electron radius. The geometrical factor $g(\theta,\phi)$ equals $\sin^2\phi$, which is in our situation can be chosen to be 1, since $\phi = 90°$ (see section 2.3.2). Integration of Eq.(2.6) and the values $\Delta\Omega = 5$ msr, $L_{det} = 1.8$ mm,$n_e = 2{\cdot}10^{19} m^{-3}$ (see section 2.3.2) give an estimation of P_s/P_0 of $1.4 \cdot 10^{-15}$. The spectral density function or dynamic form factor $S(\vec{k},\omega)$ describes the frequency shifts resulting from the individual and collective electron and ion motions. The theoretical derivation of this function is quite complicated but shows that for non relativistic velocity distributions the spectral density function can be divided into an electron and an ion term. Incoherent TS is dominated by the electron term, whereas coherent TS is dominated by the ion term. The spectral density function converges for $\alpha \longrightarrow 0$ to the assumed Maxwellian electron velocity distribution F_e in the direction of $\vec{k}$:

$$\begin{aligned} S(\vec{k},\omega)d\omega|_{\alpha\to 0} &= F_e(v_k)dv_k = F_e\left(\frac{\omega}{k}\right) d\left(\frac{\omega}{k}\right) \\ &= \frac{1}{k\sqrt{\pi} v_{th,k}} \exp\left(-\frac{\omega^2}{k^2 v_{th,k}^2}\right) d\omega, \end{aligned} \tag{2.8}$$

with v_k the electron velocity parallel to $\vec{k}$ and $v_{th,k} = \sqrt{2k_B T_e/m_e}$ the thermal velocity parallel to $\vec{k}$. Consequently, for non relativistic velocities the measured spectra are Gaussian.

In most of the tokamaks, however, the electron temperatures are so high that relativistic effects play an important role in the Thomson scattering process. For example for electron temperatures of 1 keV the value $\beta_{th} = v_{th}/c$ equals 0.06 and for 4 keV it equals 0.12. For relativistic electrons $\frac{d\sigma_T}{d\Omega}$ depends on β and, assuming an isotropic Maxwellian velocity distribution and $\theta = \phi = 90°$, the modified scattering equation can be approximated by [Mat75] [Bar89]

$$P_s(\vec{k},\lambda)\, d\lambda_s = P_0\, n_e\, L_{det}\, \Delta\Omega\, \frac{d\sigma_T}{d\Omega}\, Y \exp\left(-\left(\frac{c}{v_{th,k}}\right)^2 Z\right) d\lambda_s, \tag{2.9}$$

with

$$\frac{d\sigma_T}{d\Omega} = \frac{r_0^2}{\lambda_0\sqrt{2\pi}}\, \frac{c}{v_{th,k}}, \tag{2.10}$$

$$Y = 1 - 3.5x + 7.6x^2 - 13.3x^3, \tag{2.11}$$

$$x = \frac{\lambda_s - \lambda_0}{\lambda_0}, \tag{2.12}$$

$$Z = x^2(1-x)/2 \qquad (2.$$

and c the velocity of light. Eq.(2.9) is accurate to better than 15% for $T_e < 25$ keV and accur to better than 1% for $T_e < 2$ keV. The acquired spectrum looks like a Gaussian shifted to shorter wavelength side (the blue side) of the spectrum. For $T_e = 1$ keV the blue shift is ab 10 nm, i.e. 16% of the width $\sigma = 62nm$.

2.3.2 Thomson scattering set-up

Laser The laser, which is not shown in Fig. 2.3, is a ruby laser ($\lambda_0 = 694.3$ nm) with a maxim energy of 25 J per pulse of 15 ns. The laser consists of an oscillator cavity and three amplifi and produces a 25 mm wide beam. The beam is guided to the tokamak via mirrors and is gui vertically through the plasma and is focussed in the plasma center to a width of 1 mm. T beam width at the edges of the plasma is 2.5 mm. Below the torus the laser light is dump on a glass plate, which is placed under 45°. A $\frac{1}{2}\lambda$ retardation plate can be placed in the be somewhere near the laser to vary the polarization angle of the laser light when needed.

Detection part The radial TS set-up is shown in Fig. 2.3. The laser light that is scattered

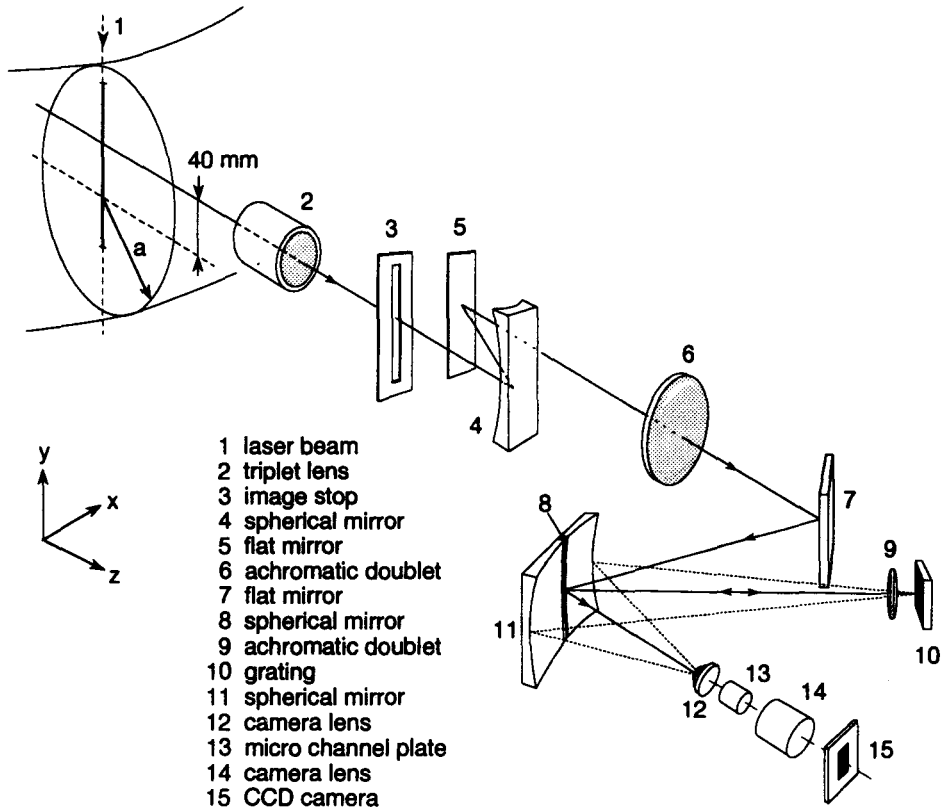

Figure 2.3: *An outline of the Thomson scattering set-up.*

the electrons in the vertical chord (Fig 2.3 nr.1, the solid line) under an angle of approximat 90° within a solid angle of 5 msr is guided via a set of lenses and mirrors (Fig. 2.3 items 2–7) a spherical mirror (item 8), which serves as the entrance slit of the Littrow polychromator (it 8–11). The grating is turned such that light with wavelength λ_0 is sent back into the plasma

the entrance slit, which suppresses the stray light considerably. Via a spherical mirror (item 11) the spectrally resolved light is imaged on a gated image intensifier with a GaAs photocathode and finally detected by a CCD camera. The area of the chip, which is divided into 384 × 576 pixels, is $10 \times 15\,mm^2$. Calibration of the system is done semi in situ with a tungsten ribbon lamp. Two slightly different TS set-ups have been used to do the measurements:

- set-up 1 (SU1), in use until September 1994: The CCD was placed in such a way that it had 576 rows of pixels in the vertical direction. In the plasma a vertical chord was observed in the range -77.2 – 124.8 mm. The spectral range was 569.2 – 818.9 nm. To gather enough scattered light 5 × 6 pixels were grouped per measuring point. This yielded 114 measuring points in the z direction of which 93 were useful and 64 in the wavelength direction of which 57 were useful, restricting the useful wavelength domain to 582.2 – 801.3 nm. Each group of pixels represented therefore 1.75 mm × 3.9 nm.

- set-up 2 (SU2), in use from September 1994 until January 1995: SU1 was changed to observe a larger part of the Thomson spectrum, which should increase the accuracy for higher temperatures. To this end the CCD camera was rotated, lenses were moved and the spherical mirror (item 11) was enlarged in the wavelength range. The observed spatial and spectral ranges were -67.6 – 126.5 mm and 397.9 – 934.9 nm resp. Grouping 3 pixels in the vertical direction and 4 in the wavelength direction gave 128 measuring points in the spatial domain, of which 113 were useful and 144 in the wavelength domain of which 82 were useful restricting the useful wavelength domain to 541.6 – 851.9 nm. Each group of pixels represented therefore 1.5 mm × 3.8 nm, on average.

Some examples of measurements carried out with SU1 are shown in Fig. 2.4.

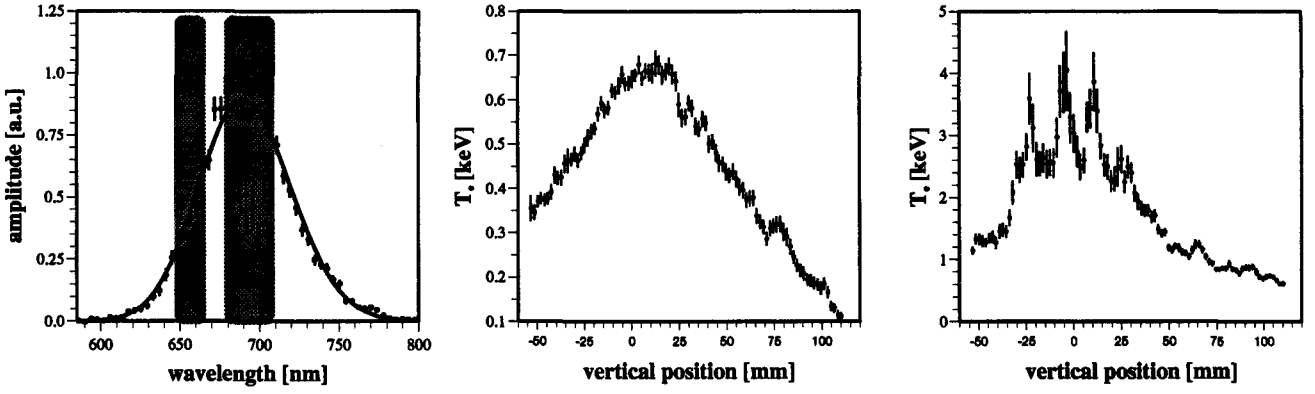

Figure 2.4: *An example of a measured spectrum (left), T_e profile measured during ohmic heating (middle), T_e profile measured during ECH heating (right). In the left picture the H_α and the laser wavelength have been cut out of the spectrum.*

background and instrument function Since SU2 is operating, only a part of the CCD chip in the wavelength direction is used. On that part of the camera on which no Thomson scattered light is falling we observe a background signal. In the time SU1 was operating there was a background signal as well, but it was not observed separately from the Thomson scattered light, because the CCD camera was used until the edges. The background signal is probably caused

by the 2-dimensional instrument function, which looks like a narrow peak with a very long ta
The height of the offset therefore depends on the total amount of light falling on the CCD chi
The best way to account for this offset is to deconvolute the signal with the instrument functio
but this is not easy, because the 2-D instrument function is not the same for every position
the CCD chip. For the moment the offset is accounted for by having the offset fitted by t
fitting program as a third free parameter. For sure this is necessary for the ohmic discharge
but in case of the ECH discharges the spectra are so wide that the offset is not visible and it
not sure that the fitting program finds the right offset. That's why the ECH discharges have n
been fitted with the offset as a free parameter. In the near future hopefully the convolution c
be implemented in the fitting program.

T_e, n_e and p_e profiles Thomson scattering yields profiles of T_e, n_e and p_e. The n_e profiles lo
much smoother than the T_e and p_e profiles. The tests will be applied to the T_e profiles instead
p_e profiles, since it is more common in thermonuclear research to look at T_e. T_e is also direct
related to thermal transport, which is one of the focal points of the research program on RT
Furthermore the T_e profiles show in general the same structures as the p_e profiles.

Chapter 3

Error estimation

For this study of structures on T_e profiles it is essential to have a good understanding of the systematical and statistical errors on T_e. In [Chu94] measurements are shown of the vessel stray light, noise created by the CCD, H_α emission and the plasma continuum radiation. Thanks to the short gating time of 40 ns these background signals are orders of magnitude lower than the Thomson scattered light. The signal to stray light ratio is measured to be 10^3 - 10^4.
The CCD noise is at least one order of magnitude lower than the TS signal and can effectively be removed from the measured signal, because it is an almost constant offset on the TS signal. Though the H_α emission is two orders of magnitude lower than the TS signal, it is of course concentrated at the wavelength 656.3 nm and still can disturb the spectrum at this frequency. Therefore the signal at this frequency is cut out of the spectrum. The plasma continuum emission is more than two orders of magnitude lower than the TS signal. These background sources hardly effect the measured spectrum. The statistical errors are mainly caused by the generation of Poisson noise in the photocathode and microchannel plate of the image intensifier.

The spectra are fitted with the relativistically corrected Gaussian (Eq. 2.10) and the errors on the fitting parameters are found by the fitting routine as described in [Bev69]. The errors found by the fitting routine are from now called the observational errors. To check the observational errors on T_e simulations have been carried out of TS spectra [Chu94]. This has only been done for SU1, but it will be done as well for SU2.

Starting with certain values for T_e and n_e the number of scattered photons could be calculated from the scattering equation Eq.(2.9), knowing the laser energy, the solid angle, the scattering length, the measured transmission of the optical system and the quantum efficiency the photocathode. The number of scattered photons reaching the image intensifier was taken as input of a Poisson random generator and thus spectra of scattered power were obtained. The fitting program calculated from this spectrum the simulated value for T_e and n_e.

By repeating this procedure 400 times per (n_e, T_e) couple a histogram could be made of the T_e values. The distribution of the T_e values appeared to have a quasi Gaussian shape. Histograms were made for 5000 (n_e, T_e) couples in the range [50 eV - 3.5 keV, $5 \cdot 10^{18}$ - $2 \cdot 10^{20}$ m^{-3}] and the relation between the width of the quasi Gaussian, i.e. the simulated error on T_e, and T_e and n_e could be described be an equation. From this equation for each measured value of T_e a simulated error can be calculated. In Fig. 3.1 these simulated errors are compared to the observed errors on T_e for a SU1 ECH plasma. The observed and simulated errors agree reasonably well.

The statistical methods described in this report have been applied to measured data as well as to simulated data. A simulated T_e profile was obtained by approximating the measured T_e and n_e profiles by smooth curves and disturbing this smooth T_e profile with a Gaussian random

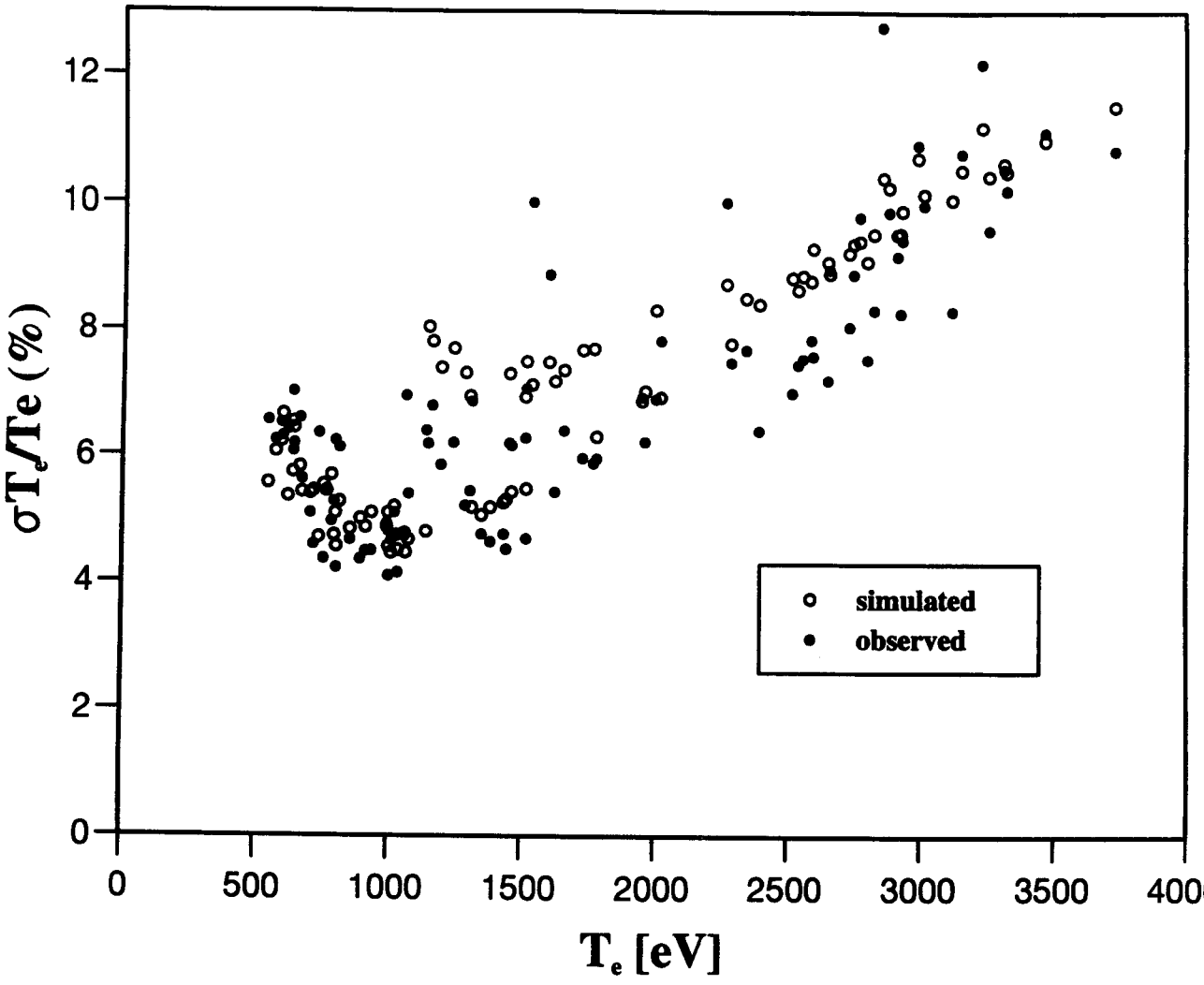

Figure 3.1: *Comparison between simulated and observed errors on Te for one of the SU1 EC plasmas.*

generator. The width of the Gaussian distribution was the simulated error on T_e.

Chapter 4

Statistical methods

To distinguish the real structures on the T_e profiles from the noise two different tools are used:

1. Power spectra. For different series of discharges the power spectra are calculated.
2. Free Knot Cubic Spline Fitting. The T_e profiles are fitted with cubic splines with free knots. The number of knots is increased and the best fit is selected with the F-test.

The two methods will be explained in chapter 4 and applied to the data in chapter 6.

4.1 Power spectra

The power spectrum of a function or set of N data points $h_k, k = 0, \ldots, N-1$, is defined as the square of the amplitude of the (discrete) Fourier transform and tells us by which sinusoidal waves the data can be reconstructed. The discrete Fourier transform (DFT) H_n is defined as

$$H_n = \frac{1}{N} \sum_{k=0}^{N-1} h_k e^{2\pi i k n/N}, \tag{4.1}$$

for the frequencies $\frac{n}{N\Delta}, n = -N/2, \ldots, N/2$, where Δ is the distance between two samples and the maximum resolved frequency $\frac{1}{2\Delta}$ is called the Nyquist frequency f_{Ny}. Equation 4.1 is periodic in n, with period N, so $H_{-n} = H_{N-n}$. Further $H_n = H^*_{-n}$, so the power spectrum is symmetric around $n = \frac{N}{2}$. The total power in the time or spatial domain is the same as the total power in the frequency domain according to Parseval's theorem:

$$\sum_{k=0}^{N-1} |h_k|^2 = N \sum_{n=0}^{N-1} |H_n|^2 \tag{4.2}$$

There are some undesired effects connected with the DFT:
1 Aliasing: The calculated power for frequency f has also a contribution from frequencies $f + nf_{Ny}$, n being an integer. As long as the power for high frequencies is low compared to the power for lower frequencies, the contribution from frequencies above the Nyquist frequency probably will also be low.
2 Finite sampling interval: The discrete data are obtained by sampling an infinite function on a finite sampling interval. This is practically the same as sampling on an infinite interval and multiplying the data with a square window, which is a function that is 1 on the sampling interval

and 0 outside. The Fourier transform of the product of 2 functions is equal to the convoluti of the Fourier transforms of the 2 individual functions according to the reversed convoluti theorem. The Fourier transform of a square function is a sinc function, so the discrete Four transform is in fact the convolution of the 'real' transform with the sinc function. Because sinc function doesn't extinguish completely for higher frequencies, the signal in all frequen channels is influenced by the signal of the neighbouring frequency channels. To decrease tl effect an other window can be applied, e.g. a triangular window, the so called Parzen windo The Fourier transform of a Parzen window drops much faster to zero and the influence of neig bouring channels stretches out to only 1 or 2 channels. In appendix A it is shown that a Parz window is needed for the considered data.

4.2 Free knot cubic spline fitting

A different technique to assess the statistical significance of structures on the profile is provid by 'Free knot cubic spline fitting' (FK). The idea behind this method is to find the best through the data, while increasing the number of free parameters. A curve with m free para eters is fitted through the data, i.e. the T_e profile, which consists of M_{data} data points. T quality of the fit is expressed by the χ^2 value, which is defined as

$$\chi^2 = \sum \left\{ \frac{1}{{\sigma_i}^2} [y_i - y(x_i)]^2 \right\}, \tag{4.}$$

where for each data point i, σ_i is the error bar, y_i is the measured value and $y(x_i)$ is the cur value. The χ^2 statistic has the following probability distribution function: [Bev69]

$$P_\chi(\chi^2, \nu) = \frac{(\chi^2)^{\frac{1}{2}(\nu-2)} e^{-\chi^2/2}}{2^{\nu/2}\Gamma(\nu/2)}. \tag{4.}$$

The gamma function is here defined as the factorial function for integral and half-integral guments and ν, the number of degrees of freedom , is defined as $M_{data} - m$. The χ^2-value i measurement of the difference between the parent function (the model) and the fitted functi as well as the deviations between the parent function and the data.

Since we are *looking* for the parent function instead of knowing it already, the χ^2-test is n a good method in this case. In fact, if the number of degrees of freedom of the fitting functi is chosen to be equal to the number of data points, χ^2 can always be put to zero, yielding function which is probably not the parent function at all. A test is needed to determine wh function approximates the underlying parent function of the data best. In a special form t F-test can do this. The F-test compares two different fits to the same data. The F-value f defined as $\chi^2_{\nu_1}/\chi^2_{\nu_2}$, with ν_1 and ν_2 the numbers of degrees of freedom for the two fitting curv The probability function P_f belonging to the F statistic is

$$P_f(f, \nu_1, \nu_2) = \frac{\Gamma[(\nu_1+\nu_2)/2]}{\Gamma(\nu_1/2)\Gamma(\nu_2/2)} \left(\frac{\nu_1}{\nu_2}\right)^{\nu_1/2} \frac{f^{1/2(\nu_1-1)}}{(1+f\nu_1/\nu_2)^{1/2(\nu_1+\nu_2)}}. \tag{4.}$$

More interesting is the integral probability $P_F(F, \nu_1, \nu_2)$

$$P_F(F, \nu_1, \nu_2) = \int_F^\infty P_f(f, \nu_1, \nu_2) df, \tag{4.}$$

which gives the probability of finding this value of F.

Test of additional term A special form of the F-test is the *test of additional term.* Out of two χ^2 statistics a new χ^2 statistic can be formed by subtracting these two χ^2 statistics [Bev69]. Therefore, the difference $\chi^2(m) - \chi^2(m+2)$ also obeys the χ^2 statistic, where m and $m+2$ are the numbers of free parameters of the two statistics, and has two degrees of freedom. A new variable F_χ following the F-distribution can be defined as

$$F_\chi = \frac{\chi^2(m) - \chi^2(m+2)}{\chi^2(m+2)/(M_{data} - m - 2)} = -\frac{\Delta\chi^2}{\chi^2_\nu}, \tag{4.7}$$

in which the numerator is a χ^2 statistic with two degrees of freedom and the denominator a χ^2 statistic with $M_{data} - m - 2$ degrees of freedom and is called reduced χ^2. This value gives the ratio between the change of the χ^2 value after fitting with two more free parameters and the reduced χ^2. If this value is low, there is little improvement in the fitting and adding another term may not be justified. According to (4.6) there is a high probability of finding a higher value of F in this case, so P_F is the probability that there is **no** improvement made.

Free knot cubic splines The fitting function was in our case a cubic spline with free knots. The fitting interval [a,b] can be divided into subintervals by a knot sequence, $a = k_0 < k_1 < \ldots < k_N = b$. A cubic spline is defined as a cubic polynomial in each subinterval, with the extra requirement that the function as well as its first and second derivatives are continuous in each interior knot $k_1, k_2, \ldots, k_{N-1}$. The number of free parameters m is $4N$–$3(N$–$1) = N$+3 for a cubic spline with fixed knots. If the positions of the knots are free parameters as well, the number of free parameters is $(N$+3$) + (N$–1$) = 2N$+2. The number of degrees of freedom of the fit is in that case $M_{data} - (2N$+2$)$. Fitting with cubic splines has advantages especially for higher numbers of free parameters (in our case 50–60), since only cubic polynomials are used. For example fitting with polynomials of higher order (higher than 10) gives often strange results: Severe oscillations of the fitted polynomial. Fitting with fixed knot cubic splines has proven to be unconditionally stable [Lan86].

In our case M_{data} is 93 for the SU1 measurements and 113 for the SU2 measurements. To be sure that the fitting program found the global minimum in most of the cases, the fitting for each number of free parameters was done 500 times, every time taking the positions of the knots of the best previous fit, disturbing them randomly and decreasing the disturbance every next of the 500 fittings. This was necessary because of the complexity of finding the minimal χ^2 value in e.g. a 50-dimensional parameter space.
An example of a typical sequence of χ^2 values, obtained by fitting one SU1 ohmic T_e profile with an increasing number of knots, is shown in Fig. 4.1a. The trend in this sequence is given by the solid line. From this line the corresponding F-values and the values of the integral probability P_F were calculated, as shown in Fig. 4.1b.

Test on the method To illustrate the way the method works, it has been applied to a set of test-data. The test profiles were obtained by sampling the function $\sin(8 \cdot 2\pi x)/(2\pi x)$ for 31 x values: $x_0 = 0.0, \ldots, x_{30} = 1.0$. From this profile nine new test profiles were derived by disturbing the data values randomly according to Gaussian distributions with nine different widths σ. The widths were 0.01, 0.03, 0.1, 0.2, 0.31, 0.81, 1.51, 2.41 and 3.51. To the nine test profiles with different disturbance levels FK has been applied and the developments of the reduced χ^2 and the probability P_F are shown in Fig. 4.2. The P_F values are found by smoothing

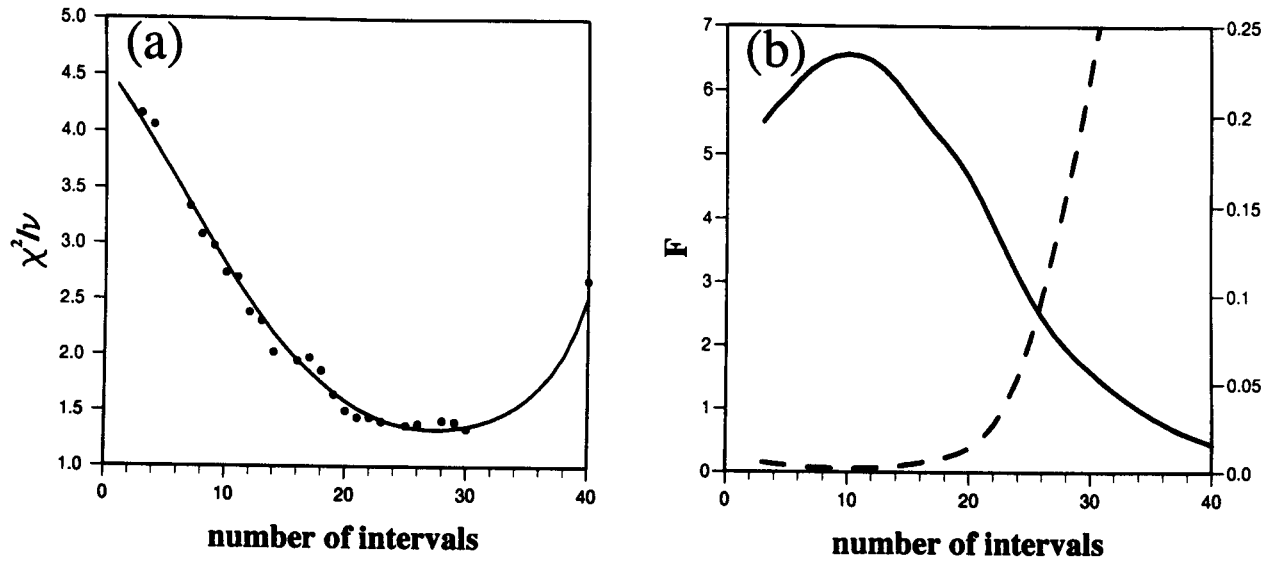

Figure 4.1: *(a) estimated χ^2_ν as a function of the number of intervals. (b) F-values (solid li and corresponding P_F (dashed line).*

the absolute χ^2 values, which are not shown in the figure. In general one can see that for three lowest disturbances χ^2_ν goes with large steps to 1, which is reached for ± 20 knots and bigger disturbances fewer intervals between the knots are needed. In most cases $\chi^2_\nu \approx 1$ for P_I 5%, which is a reason to consider the fits for 5% as the best fits.

A higher disturbance level does not always mean that there is less structure in the prof since there is a reasonable chance that the random generator creates a more structured pro for a somewhat higher σ. For example the profile with $\sigma = 1.51$ shows more structure than profile with $\sigma = 0.81$.

The profiles with $\sigma = 0.01$ and 0.03 seem to have less structure than the profile with $\sigma =$ The first two profiles, however, are very regular. The knots are almost equidistant. The fitt problem is easier for these problems and not so many knots are needed. In Fig. 4.3 the best corresponding to P_F= 5% are presented. The fits show less structure for higher disturba levels.

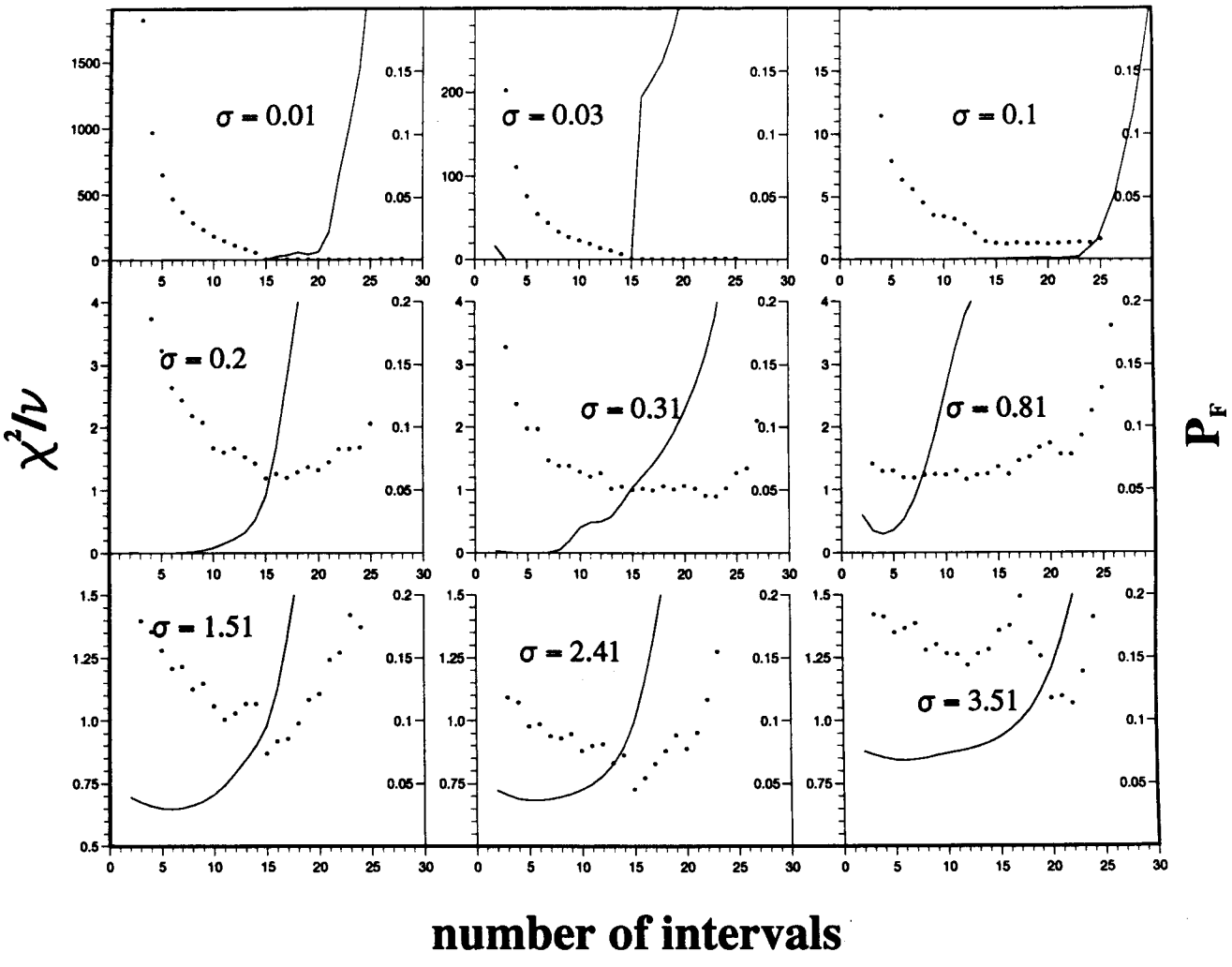

Figure 4.2: *Developments of the reduced χ^2 (indicated by the discrete points) and P_F (indicated by the solid lines) for different noise levels. The scale for the χ^2 values is on the left and the scale for P_F values on the right of each picture.*

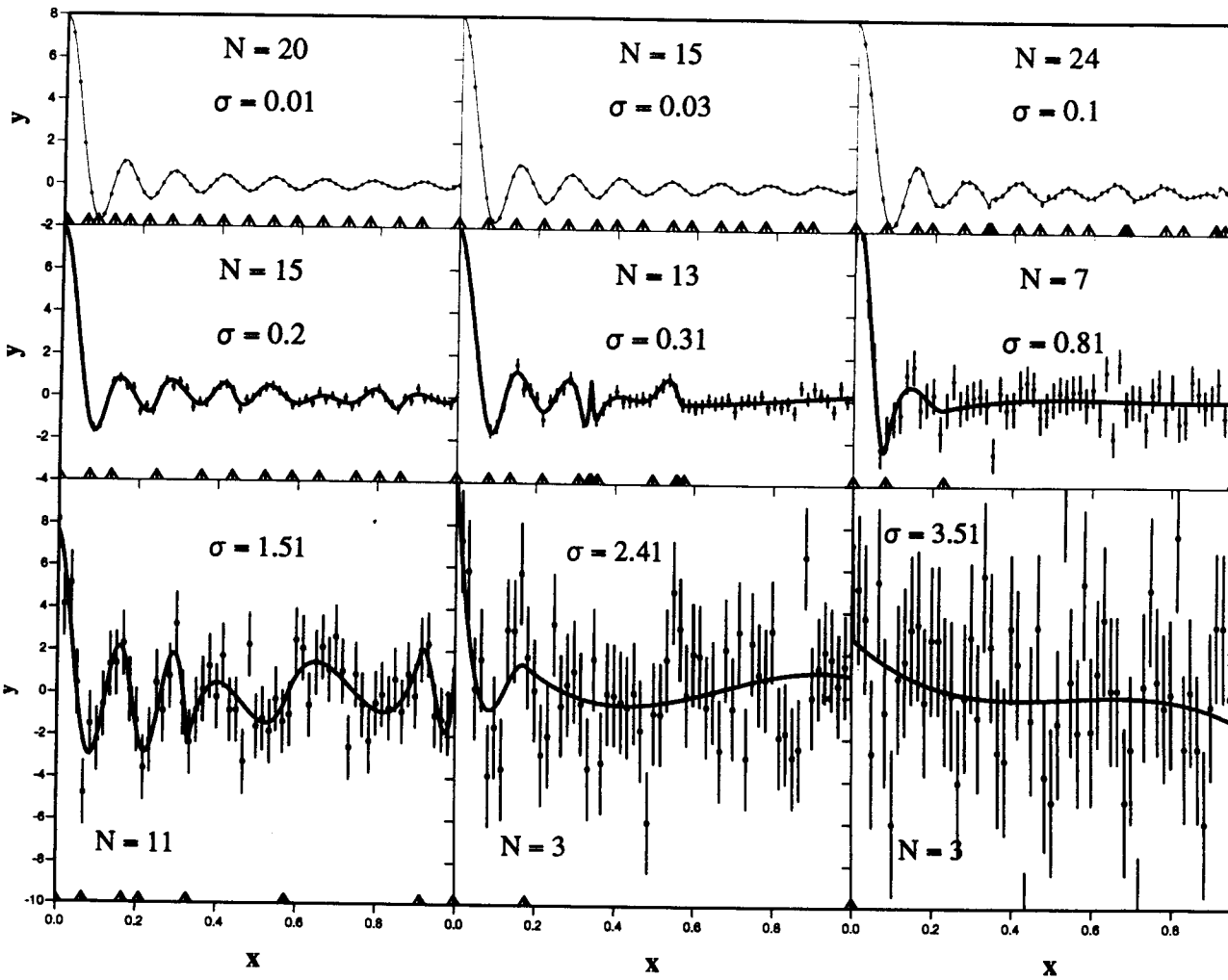

Figure 4.3: *Best fits for different noise levels. The number of intervals used for the fits is c indicated.*

Chapter 5

Data sets

The statistical analysis has been applied to 4 different data sets. For all the data sets the plasma current I_p was 60 kA, the toroidal field B_ϕ was about 2.2 T and therefore the rotational transform at the edge of the plasma q_a was approximately 7. The characteristics for the data sets are given in table 5.1. For both set-ups two data sets were created, one with ohmic heating and one with 60 GHz low field side central ECH heating. The power of the ECH was 160 kW for SU1 discharges and 130 - 140 kW for SU2 discharges. In Fig. 5.1 a typical T_e profile is shown together with the

Data set	Number of discharges	set-up	Heating	n_e(z=0)	line averaged density	T_e(z=0)	profile averaged temperature
				$[10^{19}m^{-3}]$	$[10^{19}m^{-3}]$	[eV]	[eV]
a	8	SU1	Ohmic	7.2	3.6	690	447
b	9	SU1	ECH	1.6	1.1	3000	1750
c	79	SU2	Ohmic	4.3	2.3	680	452
d	81	SU2	ECH	1.6	1.1	2300	1367

Table 5.1: *The different data sets.*

average T_e profile for each data set. The T_e profiles of data set (a) clearly show structures of $\pm$ 1 cm size, whereas the structures on the T_e profiles of data set (c) are not so clear. For the ECH discharges one observes a similar difference. The T_e profiles of data set (b) show large peaked structures $\pm$ 0.5 cm size in the middle, very hot areas where the plasma is well confined (so called filaments), sharp gradients around the sawtooth inversion radius and structures outside this radius. The T_e profiles of data set (d) show the same features, though less pronounced.

It is striking that the structures have become smaller using SU2. Especially the peaks in the center, the filaments have decreased. The difference in ECH power may have something to do with it, but the difference in power is not enough to explain the decrease. A decrease in amplitude and T_e gradients would mean that confinement in the filaments would be worse. It is therefore important to know if the decrease in amplitude is not caused by the change in Thomson scattering set up. To check if the bigger spectral range is the cause for the 'loss of structure' the spectra of the new discharges have also been fitted with the spectral range of SU1 (570 nm $< \lambda <$ 820 nm) and submitted to the same analytical methods. It will be shown in chapter 6 that the different fitting range does not introduce more structures.

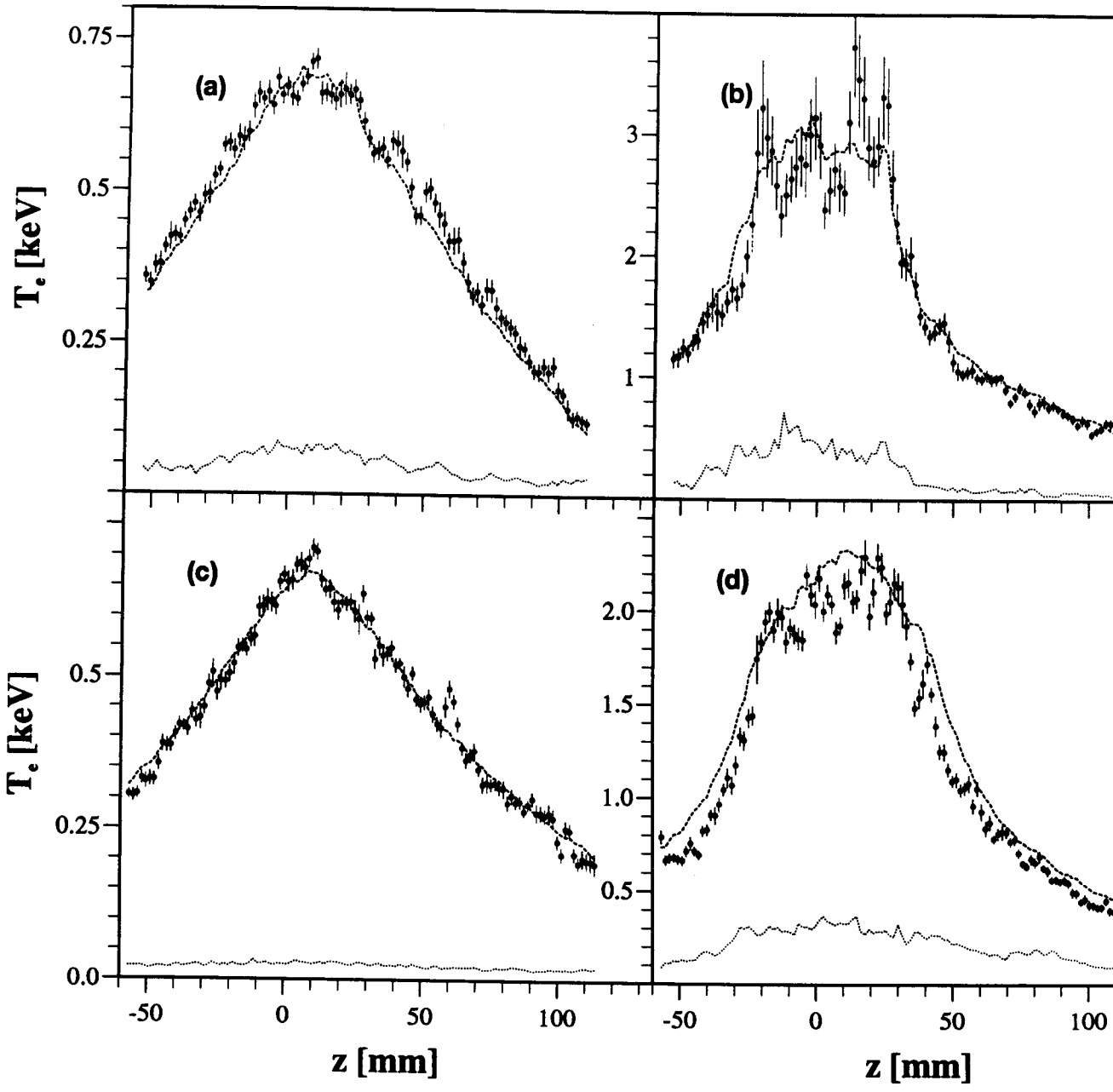

Figure 5.1: *Typical T_e profiles for the 4 data sets: data set (a), data set (b), data set (c), da set (d). In each picture the dashed line represents the average T_e profile for each data set a the dotted represents the square root of the variance of the average T_e profile.*

Chapter 6

Results

6.1 Power spectra

For all 4 data sets power spectra have been calculated by averaging the power spectra of the individual T_e profiles in each data set. To decrease the window effects, the average of each T_e profile has been subtracted from the profiles (this filters out the very high zero frequency, which would give a leakage into other frequency channels, see appendix A) and the profiles have been multiplied by a Parzen window. In Fig. 6.1 a comparison is made between the ohmic and the ECH discharges for each set-up and in Fig. 6.2 a comparison is made between the discharges of the two set-ups.

Comparison ECH – Ohmic – simulations In Fig. 6.1a the power spectra are shown for the SU1 data sets together with the power spectra of the simulated data, indicating the simulated noise level. For the noise level of the ohmic discharges 80 simulated T_e profiles were used and 45 simulated T_e profiles were used for the noise level of the ECH discharges. For lower spatial frequencies the signal is well above the noise level. This is an indication that the T_e profiles for the ohmic and ECH discharges certainly have low frequency structures (wavelengths longer than 1 cm). The power spectrum of the simulated noise for the ohmic discharges shows some low frequency peaks. They are caused by windowing effects. For higher frequencies the signal for the ohmic data set almost coincides with the noise level, whereas the high frequency signal for the ECH data set is 6× lower than the noise level, which is quite remarkable. This is discussed below.
For the SU2 data sets (6.1b) the signal is also higher for lower frequencies (about 10×), indicating that low frequency structures are present in the T_e profiles of about the same size as in the ohmic T_e profiles. Although simulations have not been carried out for SU2 yet, it is expected that the shape of the power spectra for these simulations will be very similar to the power spectra of the simulations for SU1. In Fig. 6.1a the ratio between the ECH and the ohmic power spectra is about 250 for lower frequencies and about 60 for higher frequencies. Because power spectra are the square of the Fourier spectra this means that the square root should be taken of these ratios to connect it to T_e values, which gives factors 16 and 8. In Fig. 6.1b these factors are 7.5 and 6.5 for lower and higher frequencies resp.

The high simulated noise level cannot be correct, so there must be something wrong with the simulations. The formula used for the simulations (see chapter 3) might not be correct for high frequencies. The simulated errors on T_e that are calculated with this formula, however, agree with the observed errors on the measured T_e (Fig. 3.1). So the simulations are probably correct.

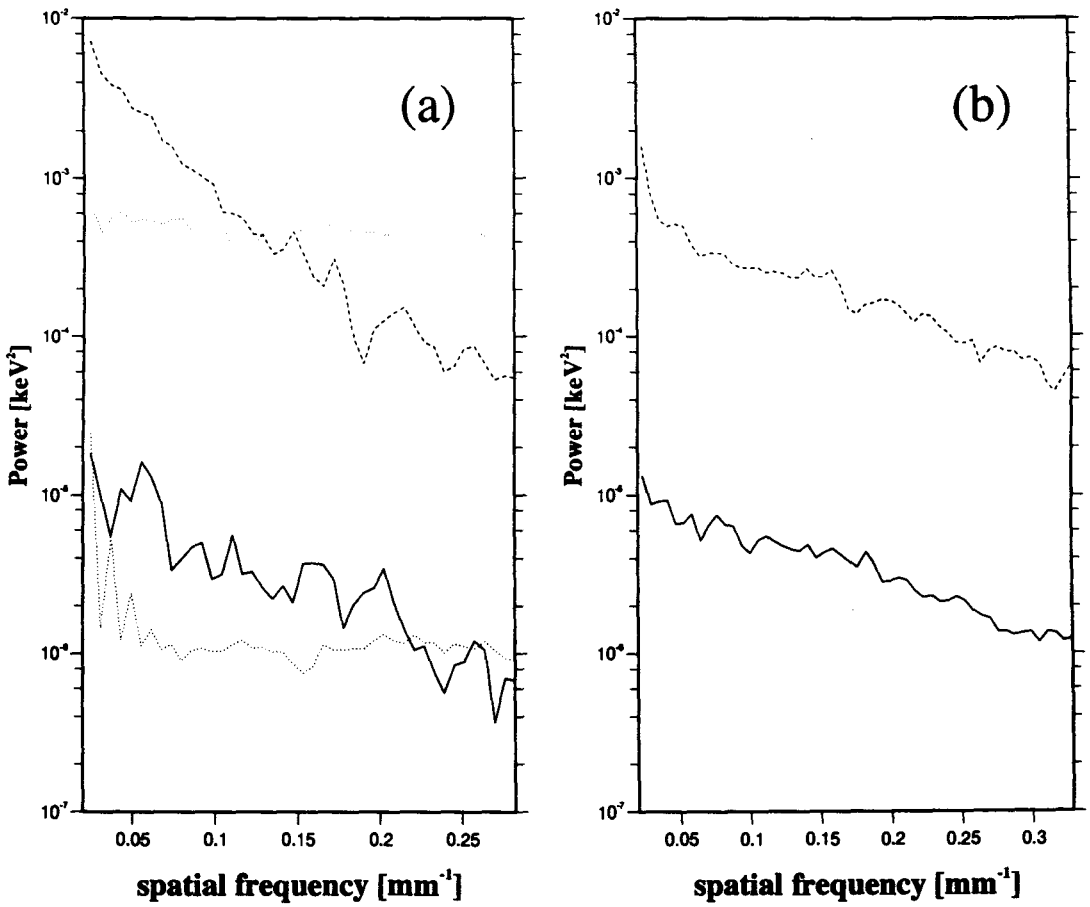

Figure 6.1: *(Absolute) Power spectra for the SU1 (a) and SU2 (b). In the upper parts the l power spectra are shown (dashed lines) and in the lower parts the ohmic (solid lines). For the power spectra for the simulated discharges are given by the dotted lines.*

The input values for the formula (the smooth T_e and n_e profiles) might be wrong, but to acc for the high noise level for example the values for n_e should be 3 times lower, which is far be the error bars. Besides that, the fact that the simulated errors on T_e agree with the obse errors argues against this option.
Another possibility might be that convolution of the real TS signal on the CCD with the ins ment function smoothes the signal, so that Thomson scattered light spectra are correlated the neighbouring spectra. In this way the higher spatial frequencies are filtered out of th profiles. If this were the case, however, one would expect a stronger decrease for higher freq cies, as if it were a high frequency filter. To check if this is the cause of the discrepancy simulations should be done including the instrument function. For SU1, however, the instru function is not known for every position.
For the moment we cannot be sure about the reason for the high simulated noise level.

The gap between the power spectra for the ohmic and ECH profiles for SU1 can be expla as follows: From the average T_e values of table 5.1 it can be seen that on average the ECH pr are 4 times higher than the ohmic profiles. This gives a T_e scaling factor of 4. The fact structures on the ECH profiles are bigger also after scaling to ohmic temperatures gives a f 2 for lower frequencies. The use of a Parzen window gives another factor 2, because the Pa

window emphasizes the middle of the profile (the hottest part), the part where the structures and the noise are biggest for the ECH discharges. So for low frequencies the ratio between the ECH spectra and the ohmic spectra is $4 \times 2 \times 2 = 16$ and for high frequencies it is $4 \times 2 = 8$. For SU2 temperature scaling gives a factor 3, the bigger structures and higher noise level for ECH discharges gives a factor of about 1.5, the remaining factor of about 1.5 comes from the use of the Parzen window.

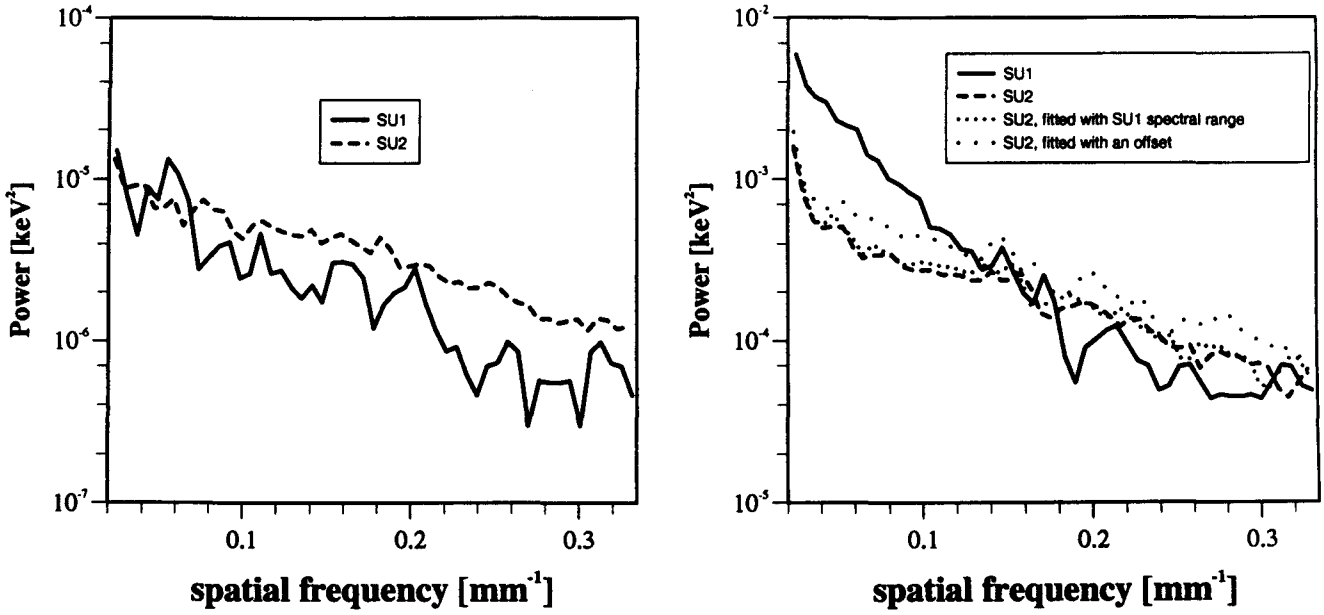

Figure 6.2: *(a) Comparison ohmic power spectra for SU1 and SU2. (b) Comparison of ECH power spectra for SU1, SU2 and refitted profiles.*

Comparison SU1 – SU2 The power spectra of Fig. 6.1a and Fig. 6.1b cannot be compared directly, since the units on the frequency scale are slightly different and the SU2 power spectra contain more points (113 vs. 93). For direct comparison the power spectra have been plotted on the same frequency scale in Fig. 6.2 and the SU1 power spectra have been multiplied by $\frac{113}{93}$, which follows from Parseval's theorem (Eq. 4.2).
Figure 6.2a shows that for the ohmic discharges of SU2 the power signal is 2–3 × higher for high frequencies than the signal for SU1.
Figure 6.2b shows the power spectra for the ECH data sets. Most striking is the fact that for lower frequencies the power spectrum for SU1 is about 4× higher than the power spectrum for SU2. The main difference between the 2 set-ups is the observed spectral range, so by fitting the spectra of SU2 in the fitting range of SU1 one can easily check if the change in spectral range is responsible for the loss of structures, already mentioned in chapter 5. The result is shown in Fig. 6.2b: a 10% increase of the spectrum. Further, the spectra were fitted with an offset as a third free parameter (see section 2.3.2). This gave a 30 – 40% increase of the spectrum.

The fact that the high frequency signal for the ohmic discharges differs by a factor 2–3 can be explained by the fact that the SU2 data set was obtained during lower density discharges (average $n_e(0) = 7.2 \cdot 10^{19}$ for discharges for SU1 and $4.3 \cdot 10^{19} m^{-3}$ for SU2). So the noise level for the SU2 discharges is higher. If one assumes that the simulations are also valid for SU2, one

can calculate that the noise level for the SU2 ohmic discharges should be 2× higher than the level for SU1 ohmic discharges.

The factor 4 difference in low frequency power signal for the ECH data sets can partly be explained by the fact that the SU1 T_e profiles were 1.3 times higher than the SU2 T_e profiles because of difference in applied ECH power of 20%. This gives a factor $1.3^2 \approx 1.6$ difference in power signal. This still leaves a factor 2.4 in power signal which cannot be compensated for by the 10% higher power signal for the SU2 profiles fitted with the SU1 spectral range. Neither can the 30% higher power signal of the SU2 profiles fitted with an offset. It is also disputable if the structures that have grown by fitting with an offset are real, since the offset shouldn't be a free parameter, but something determined by the total or local amount of light falling on the CCD camera. A factor 2.4 difference in power signal means that the structures/filaments are on average 50% bigger for SU1. This was also visible in Fig. 5.1b-d, the T_e profiles of SU1 showed much higher peaks than the T_e profiles of SU2. Probably the loss of structures is not caused by the change in TS set-up, but by a change of the plasma itself. It could for example depend on the purity of the plasma. However for both SU1 and SU2 the value of Z_{eff} was about 2.6.

6.2 Free knot cubic spline fitting

With the method of free knot cubic spline fitting, the significance of structures can also be shown. Furthermore one can get an idea of the shape of the structures. Unfortunately FK generally consumes a lot of CPU time: one T_e profile takes about 12 hours CPU time. For this reason it has not been applied to all T_e profiles, but only to a selection. The method has been applied to all 8 T_e profiles of data set (a) (ohmic SU1), 4 profiles of data set (c) (ohmic SU2), 4 simulated ohmic SU1 T_e profiles and 4 profiles of data set (b) (ECH SU1).

Ohmic SU1 discharges In Fig. 6.3 the results of the fitting are shown for 4 ohmic SU1 T_e profiles out of a series of 8 fitted T_e profiles. The number of intervals between the knots needed is 20 – 24 for a probability of 5% of **no** improvement in the fitting sequence. The best fits corresponding to these numbers of intervals (Fig. 6.3b) show that structures of size down to 1 cm are fitted.

Ohmic SU2 discharges In Fig. 6.4 the results are shown for 4 ohmic T_e profiles measured with SU2. The number of intervals needed is varying from 15 to 25. Two of the profiles are as structured as the profiles of SU1 and two are less structured. It seems that the structure of the SU2 profiles varies more than the structure on SU1 profiles, though the number of four discharges is not enough to be sure of that.

Simulated ohmic SU1 measurements Simulated profiles for the same average T_e and n profiles as the ohmic discharges of SU1 have been fitted as well and need 1–10 intervals between the knots for 5% probability of no improvement, as shown in 6.5. Furthermore the lines representing P_F are not as steep as in Fig. 6.3. In other words already in the beginning the program does not find big improvements in the fitting for each step. The fact that the simulated discharges need fewer knots proves again that the T_e profiles of the ohmic discharges contain structures not created by noise.

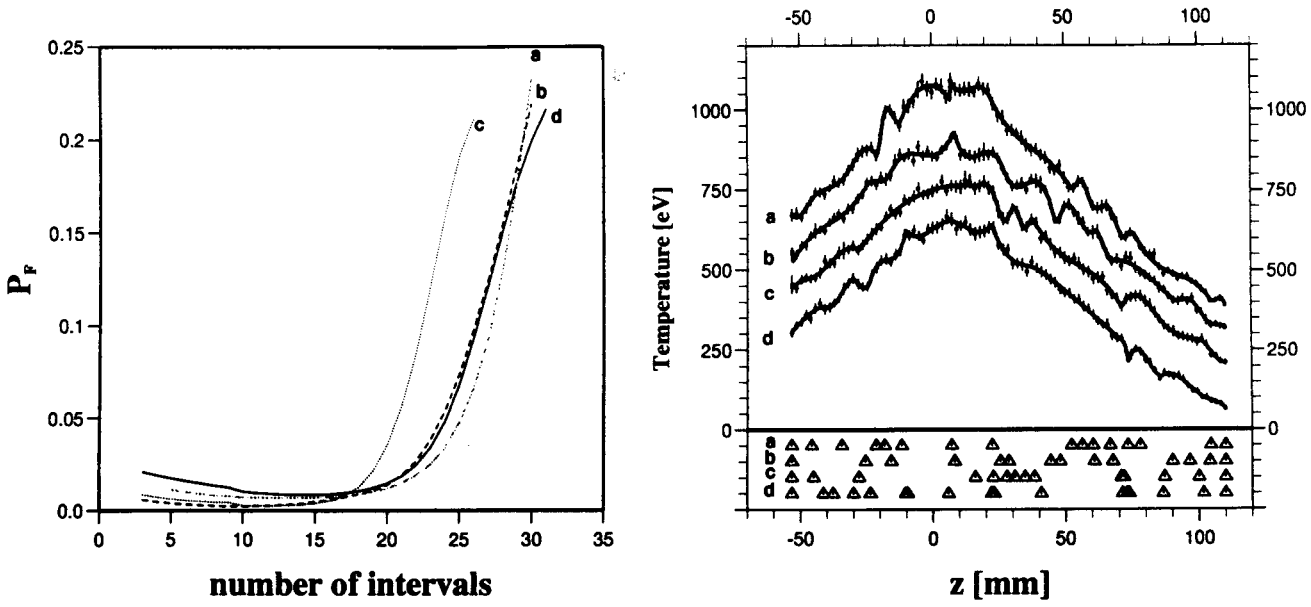

Figure 6.3: *(a) P_F versus number intervals for four different ohmic plasma discharges measured with SU1. (b) Best fits for four different ohmic plasma discharges. For the curves a – d 24, 19, 21 and 22 intervals between the knots were used. The triangles indicate the positions of the knots. The curves a – c are shifted up 300 eV, 200 eV, 100 eV respectively. Structures of about 1 cm are fitted.*

ECH SU2 discharges Finally 5 ECH discharges of SU1 have been investigated. To save computing time the T_e profiles have been divided into 2 parts: The central, filamentary part and the edge part, with structures that look like the structures on ohmic T_e profiles. The resulting probabilities for the central part are shown in Fig. 6.6a and for the edge part in Fig. 6.6b. The best fits for the central and edge parts are both shown in Fig. 6.7. From the best fits it appears that both the filaments and the edge structures are significant. The number of knots needed per cm for the central part varies from 0.4 for discharge d, which does not show any structures to 1.7 for discharge b. The number of knots needed per cm for the edge part varies from 0.9 for discharge a to 1.6 for discharge b.

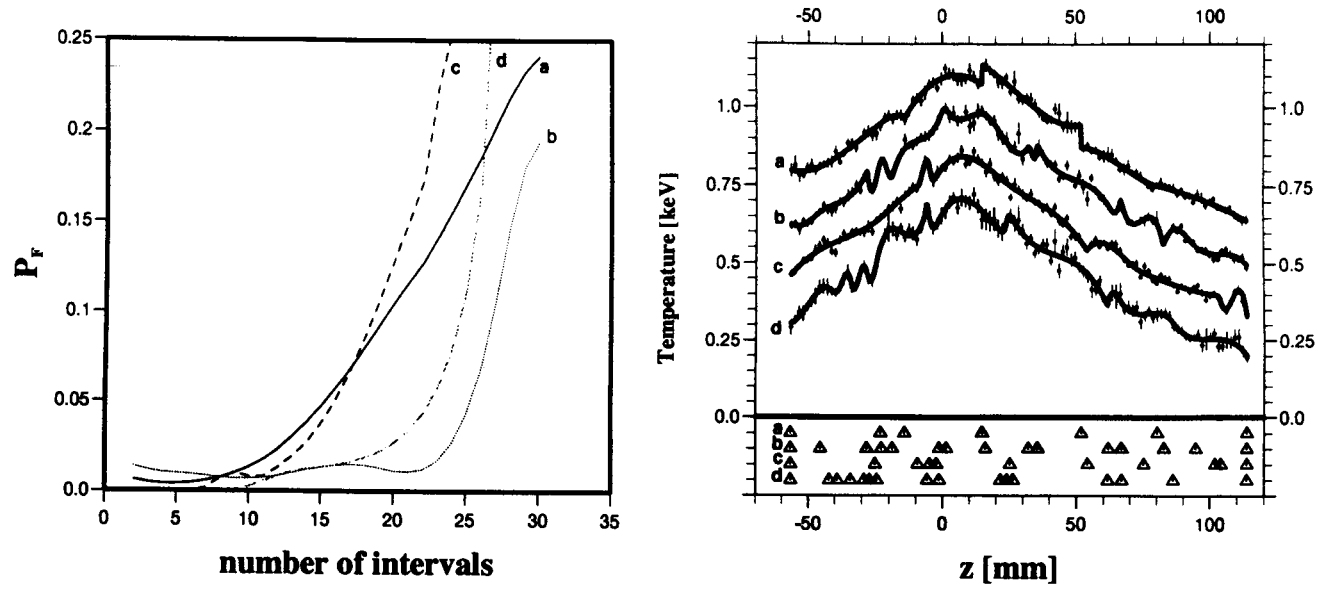

Figure 6.4: *P_F and corresponding best fits for 4 ohmic discharges measured with SU2. For the curves a – d 15, 25, 16, 22 intervals between the knots were used. The curves a – c are shifted up 450 eV, 300 eV, 150 eV respectively. Structures of about 1 cm (some even of 0.5 cm) are fitted.*

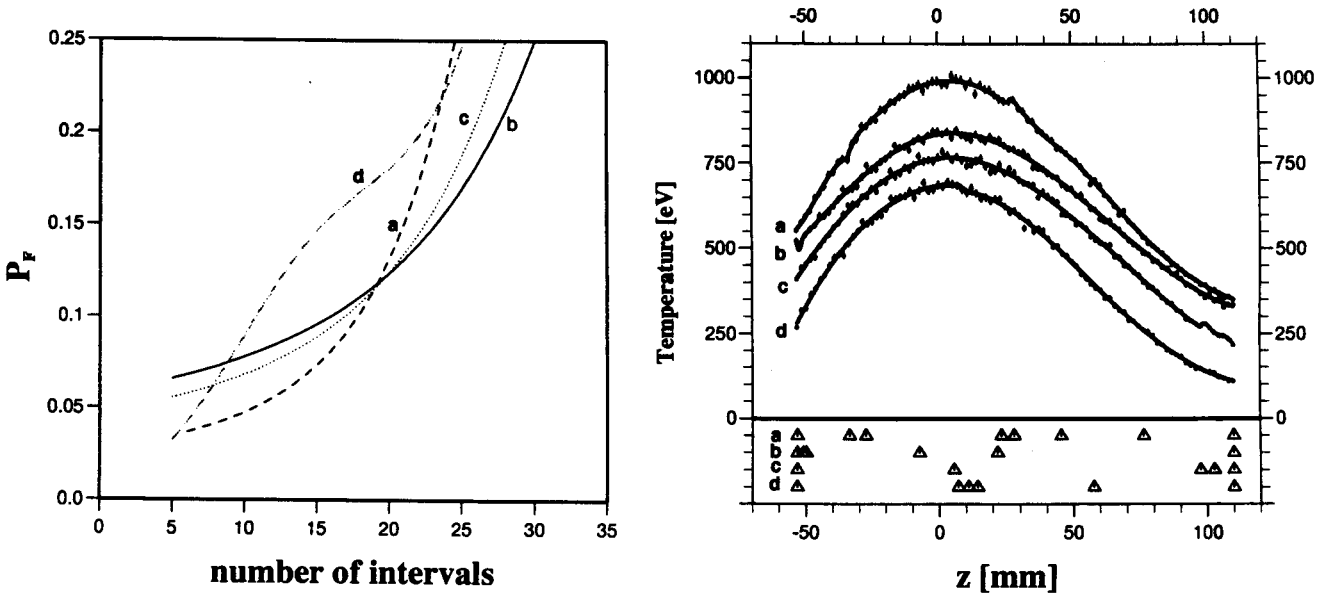

Figure 6.5: *(a) P_F-values for simulated discharges. (b) profiles for simulated discharges. The curves a – c are shifted up 300 eV, 200 eV, 100 eV respectively. It is shown that for simulated data very few structures are found.*

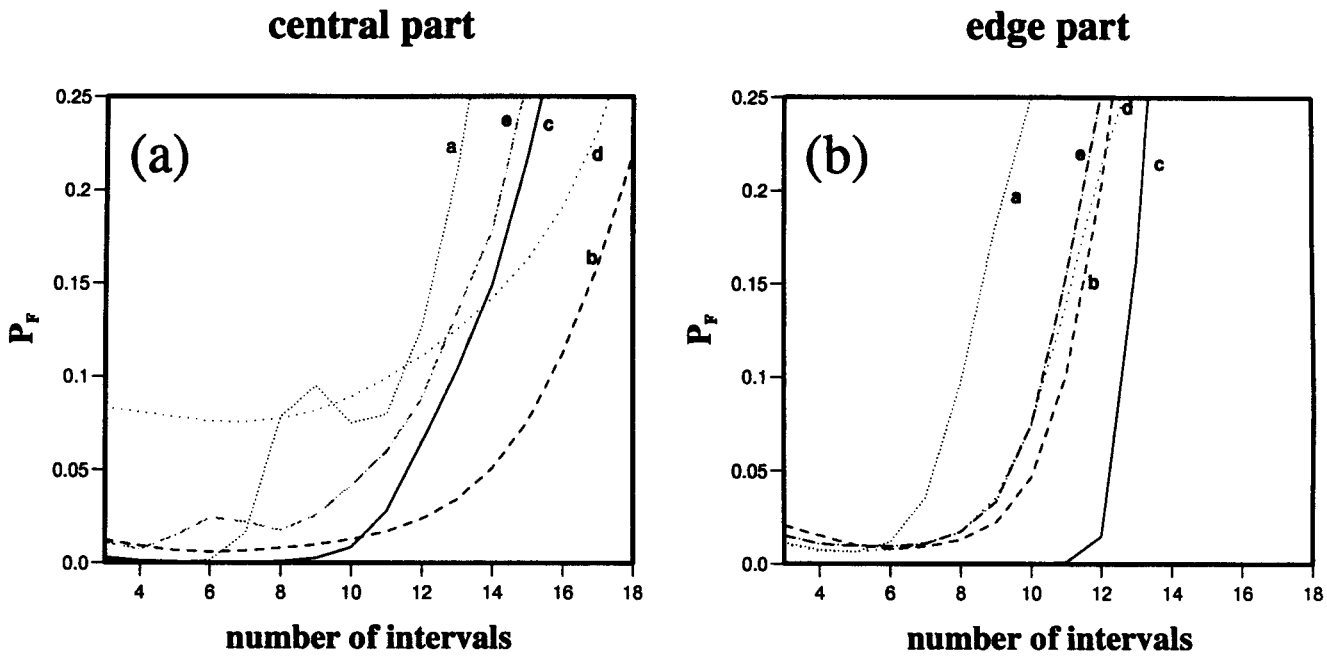

Figure 6.6: *P_F 5 ECH discharges of SU1, central part (a) and edge part (b). The total number of intervals needed for a confidence interval of 95% is about the same as for the ohmic SU1 discharges:* ± 20.

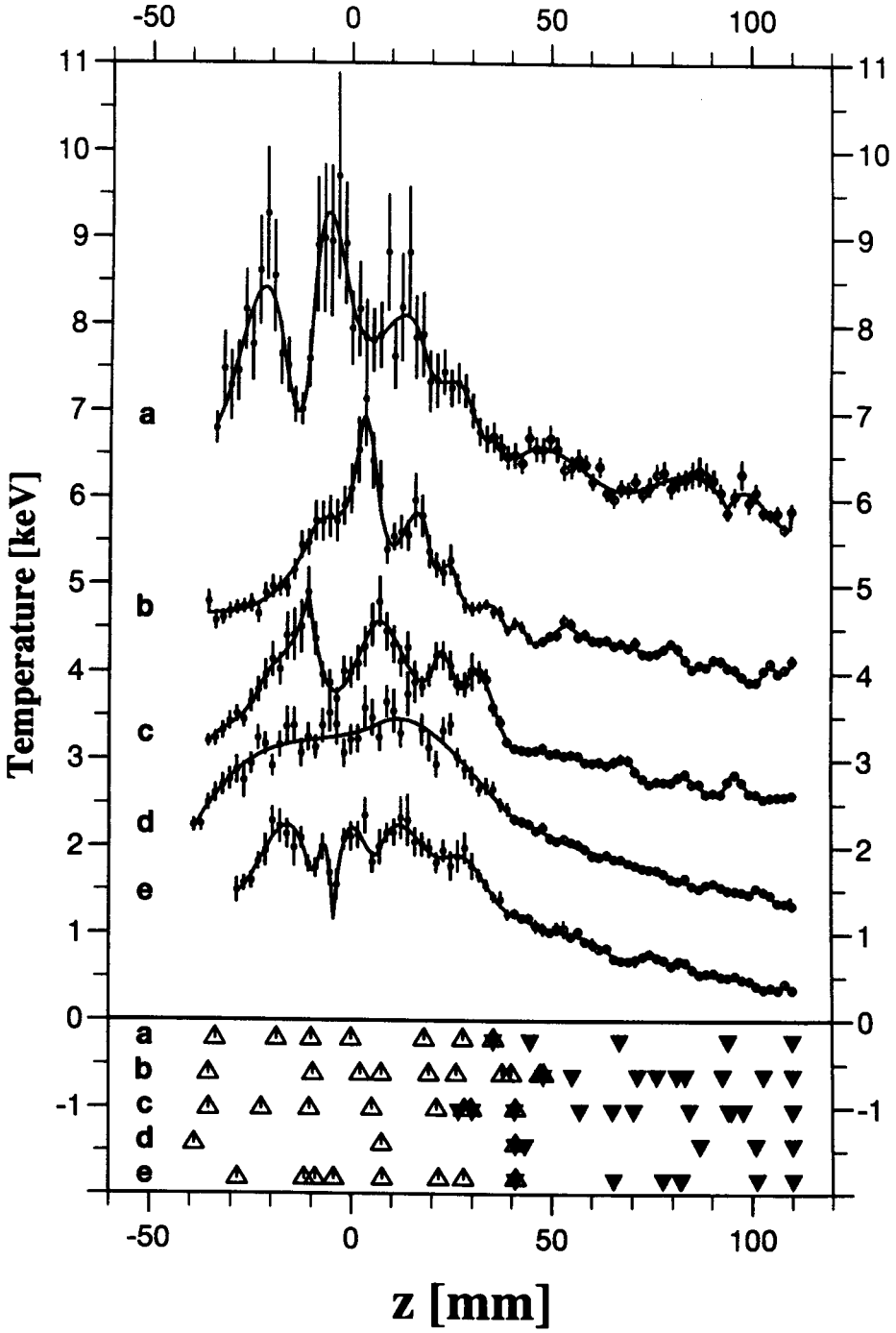

Figure 6.7: *The best fits corresponding to $P_F = 5\%$, for both the central and edge part. The solid triangles show the knot positions for the edge part and the open triangles show the knot positions for the central part. The curves a – d have been shifted up 5, 3.5, 2 and 1 keV respectively. The number of data points used for the fitting was for the central parts of profiles a – e 40, 48, 44, 46 and 40 resp. and for the edge part 43, 36, 48, 40 and 40 resp. The number of intervals between the knots used in the fits was for the central part 8, 14, 12, 3 and 10 and for the edge part 7, 10, 12, 9 and 9.*

Chapter 7

Summary and Discussion

The results of chapter 6 can be summarized as follows:

- The power spectra of T_e profiles of ohmic and ECH discharges are for low frequencies well above noise level, implying low frequency structures.
- The difference in signal for high frequency between the ohmic discharges of SU1 and SU2 can be explained by a difference in n_e.
- The ECH discharges of SU1 have, however, a 6 $\times$ higher signal for lower frequencies than the ECH discharges of SU2, while the plasma conditions were practically the same.
- Refitting the SU2 ECH spectra with the spectral range of SU1 hardly changes the power spectrum. Fitting with an offset as third parameter gives a power spectrum which is a little bit higher but not high enough to account for the gap between the power spectra for SU1 and SU2 at low frequency.
- For that reason the 'loss of structures' cannot be attributed to the change in TS set-up. Besides the fact that the applied ECH power was 15% lower for the SU2 ECH discharges, the plasma itself may have changed in the sense of having e.g. a lower or higher value for Z_{eff}.
- FK showed that 20 – 25 knots are sufficient to get the best fits with a confidence level of 95% for the high density ohmic discharges, measured with SU1. This can be related to a structure size down to 1 cm.
- The simulated profiles (smooth profiles with simulated noise) needed 1 – 10 knots and therefore show hardly any structure.
- The ohmic discharges measured with SU2 showed a wider variation in structure than the SU1 discharges, because 15 – 25 knots were needed.
- The SU1 ECH discharges show large structures in the central part, the so called filaments.

What can be learnt from the results?
From the results it appears that the observed deviations from the smooth profiles are not artefacts created by the Thomson scattering diagnostic. The significant structures observed on ohmic T_e profiles have a size of about 1 cm or bigger. Smaller structures disappear in the noise. The size of

the filaments is about 0.5 – 1 cm. The observed shape of the T_e (and p_e) profiles agrees very we with the idea that the magnetic topology can be represented by small scale filamented structure in the center and towards the edge of the plasma by rational q-surfaces that are broken up t form magnetic islands surrounded by regions of stochastic field. The measurements, however, d not *prove* this idea. For this, at least the correlation should be found between the q-surfaces an the observed structures.

One might think that the observed structures on the T_e and p_e profiles are caused by som irregularities on the mirrors and/or the CCD camera. If this were the case, the structures woul appear on the same positions for every discharge and this is not observed. The structures chang from position every discharge and if the plasma shifts downwards, the measured profile shift also.

Some restrictions of the analytical methods that have been used:

- Both FK and PS cannot directly say something about the location of the structures. FK however, gives the shape of the structures in the T_e profiles and from the derivative of th fitted splines the positions of the structures can be determined.
- Application of FK to 1 T_e profile takes on average 12 hours CPU time. This limits th applicability of the method to larger data sets.
- The FK fitting program does still not always find the absolute minimum.
- The SU2 Thomson scattering spectra have not been fitted in the best way possible, th spectra should have been deconvoluted with the instrument function.

Are there other ways of measuring this kind of structures in the plasma? Assuming that th measured bumps are in fact fluctuations ($\tilde{T}_e \approx 5 - 10\%$ for ohmic discharges and $\tilde{T}_e \approx 15 - 30\%$ for ECH discharges) one would expect to see them also with diagnostics that have high tim resolution, for example with ECE. In RTP the fluctuations have not been observed. The spati resolution is not high enough because the plasma is in the observed frequency range optical thin and the fluctuations are averaged out. Also at TFTR similar observations were done a TFTR with TS, but could not be supported by experiments done with ECE [Zar93].
At TEXT-U measurements of core fluctuations have been done by estimating the correlatio between two ECE signals originating from mostly overlapping plasma volumes [Cim95]. Th measured value for $\tilde{T}_e$ was, however, much lower: 0.5 % in the center of the plasma.
With tomographic methods such as soft X-ray tomography it might be possible to see structur in the plasma. A disadvantage of the method is that the measured signal is line-integrated, that the signal should be e.g. Abel inverted to get a radially resolved picture. By Abel inverti the signal, assumptions are made about symmetry and so the interpretaton of the signal very difficult. With the soft X-ray and visible light tomographic systems operating at RTP structures have been found, for the time being.
At RTP photos have been made of the plasma during pellet injection. The photos showed lo filamentary structures in the toroidal direction. The idea is that the cold particles hit a filamen where they are well confined and cool the whole filament because of the good toroidal transpo The cooled filament emits H_α light.
Many other experiments give also evidence for small scaled structures, e.g. experiments at JE with the LIDAR TS diagnostic showed bumpy T_e profiles, associated with magnetic islands low rationality [Nav92].

What can be done in the future with Thomson scattering ?
More discharges with different plasma parameters should be investigated with both FK and PS, so that something can be said about size and occurrence of the structures.
Maybe the discrepancy between the SU1 and SU2 discharges can be investigated further by looking at more plasma parameters, such as Z_{eff}.
An estimate could be made of the location of the structures by taking the points where the derivative of the fitted cubic splines is equal to zero or reaches a minimum. Another way is by making histograms of the knot positions (more discharges should be investigated for that with FK, e.g. 10 discharges) and possibly a link could be made between the knot positions and the rational q-surfaces, which can be measured with polarimetry in the future.
Another technique, Singular Value Decomposition (SVD), can hopefully be used in the future to effectively remove the noise from the signal at the CCD. It is much easier to use this technique for large data sets than the technique of free knot cubic spline fitting, because it takes just a few seconds CPU time to handle one discharge.
The signal on the CCD should be deconvoluted with the instrument function.
Within a year it will be possible to have two laser pulses during one plasma discharge, and in this way an estimation of the time correlation can be made and the behaviour of the filaments in time can be followed.
Recently it has also become possible to measure in the tangential direction (i.e. in the direction of the toroidal field), in which case the polarization of the laser light must be rotated

Bibliography

[Bar89] C.J. Barth. *Thomson scattering measurements of the electron velocity distribution function in the TORTUR tokamak.* PhD thesis, Rijksuniversiteit Utrecht, 1989.

[Bev69] P. R. Bevington. *Data Reduction and Error Analysis for the Physical Sciences.* McGraw-Hill Book Company, New York, 1969.

[Chu94] C.C. Chu, C.J. Barth, A.J.H. Donné, B.J.J. Grobben, N.J. Lopes Cardozo, F.J. Pijper, G.C.H.M. Verhaag and the RTP-team. High Spatial Resolution Multiposition Thomson Scattering System on RTP. In *21st EPS Conference on Controlled Fusion and Plasma Physics*, volume 18B, Part III of *Europhysics Conference Abstracts*, pages 1248–1251, Montpellier, 1994. The European Physical Society.

[Cim95] G. Cima et al. Core temperature fluctuations and related heat transport in the Texas Experimental Tokamak-Upgrade. *Phys. Plasmas*, 2(3):720–726, 1995.

[Lan86] Peter Lancaster and Kęstutis Šalkauskas. *Curve and Surface Fitting.* Academic Press, London, 1986.

[Lop94] N.J. Lopes Cardozo, F.C. Schüller, C.J. Barth, C.C. Chu, F.J. Pijper, J. Lok and A.A.M. Oomens. Plasma Filamentation in the Rijnhuizen Tokamak RTP. *Physical Review Letters*, 73(2):256–259, 1994.

[Mat75] M. Mattioli and R. Papoular. Analysis of Light Scattering Data from Relativistic Plasmas. *Plasma Physics*, 17:165–172, 1975.

[Nav92] M.F.F. Nave et al. *Nuclear Fusion*, 32:825, 1992.

[Pre86] W.H. Press, B.P. Flannery, S.A. Teukolsky, W.T. Vetterling. *Numerical Recipes.* Cambridge University Press, Cambridge, 1986.

[San91] M.C.M. van de Sanden. *The expanding plasma jet: experiments and model*, PhD thesis Technische Universiteit Eindhoven, 1991.

[She75] J. Sheffield. *Plasma Scattering of Electromagnetic Radiation.* Academic Press, New York, 1975.

[Zar93] M.C. Zarnstorff et al. In *Varenna Workshop on Local Transport in Fusion Plasmas* 1993.

Appendix A

Tests on power spectra

Before calculation of the power spectra of section 6.1 the data were multiplied by a Parzen window. In this appendix it will be explained why this was done.
In Fig. A.1 three windows are shown: a square window, a Parzen window and a Welch window.
There are of course more windows described in the literature, but the effect of these windows is

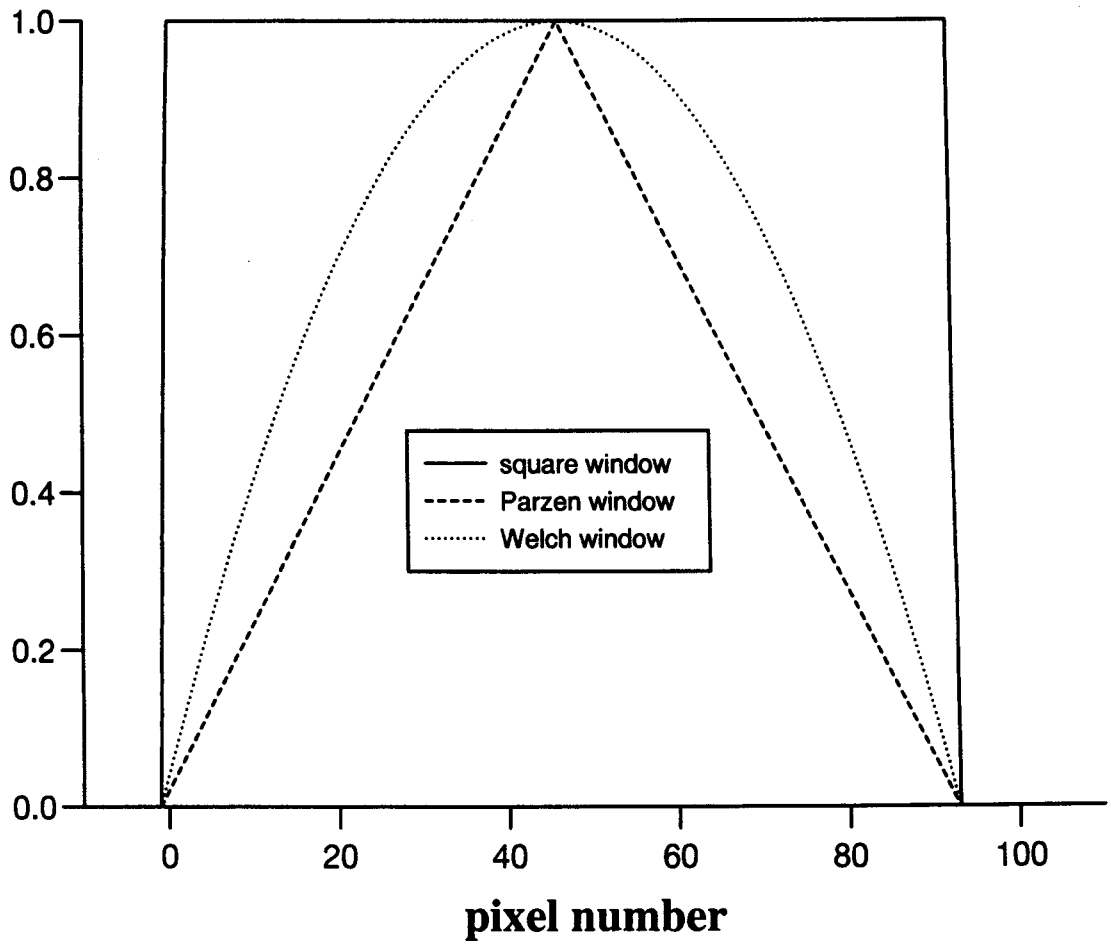

Figure A.1: *different windows: square, Parzen, Welch.*

the same: making the edges of the square window less sharp. The square of the discrete Fourier transform of a window is called leakage function and gives the amplitude with which signal from

one frequency channel 'leaks' into neighbouring frequency channels (see for example [Pre86]) The leakage function of a square window looks like the square of a sinc function and its FWHM is 1.1 channel. The FWHM of the leakage functions of the Parzen and Welch windows is abou 1.7 channels, but they extinguish much faster. In Fig. A.2 the power spectrum for the 8 ohmi discharges is shown for the three different windows. The high peak comes from the averag

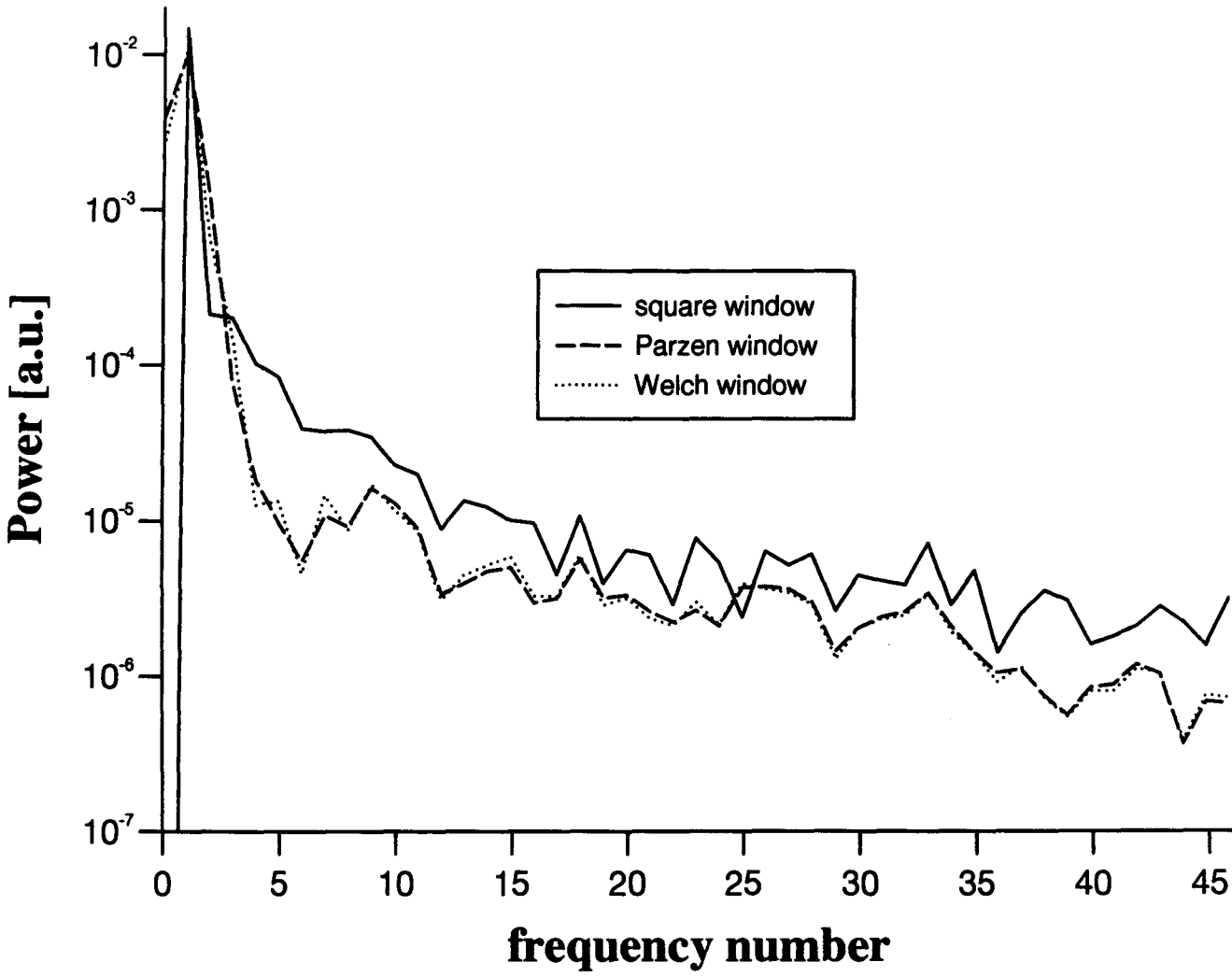

Figure A.2: *The effect of windowing on the power spectra.*

shape of the T_e profiles and is almost two orders of magnitude higher than the signal of the highe frequency channels. In case of the square window the low frequency peak disturbs the signal c up to 10 following channels, because the leakage function is for the 10^{th} frequency channel sti 10^{-3} (see formula for leakage function of square window in [Pre86]). This means a disturbanc of 10^{-2}(signal of the peak) $\times$ 10^{-3} = 10^{-5}, which is about the order of magnitude of the signa at the 10^{th} channel.

The Welch and Parzen window have almost the same effect. Here the disturbance of the hig peak stretches out to only 2 or 3 channels.

Windowing is necessary because of the low frequency peak. If, instead of windowing, the smooth global profile is subtracted from the T_e profiles, the peak will disappear and the power spectrur of the deviations is obtained. In this case a window is not needed.

One way of estimating the global profile is by fitting a function through the T_e profile. In Fig. A.3 this is done with fixed knot cubic splines with 3, 5 and 7 intervals between the knots, which means 6, 8 and 10 free parameters respectively. In this way only the low frequency part of the profiles

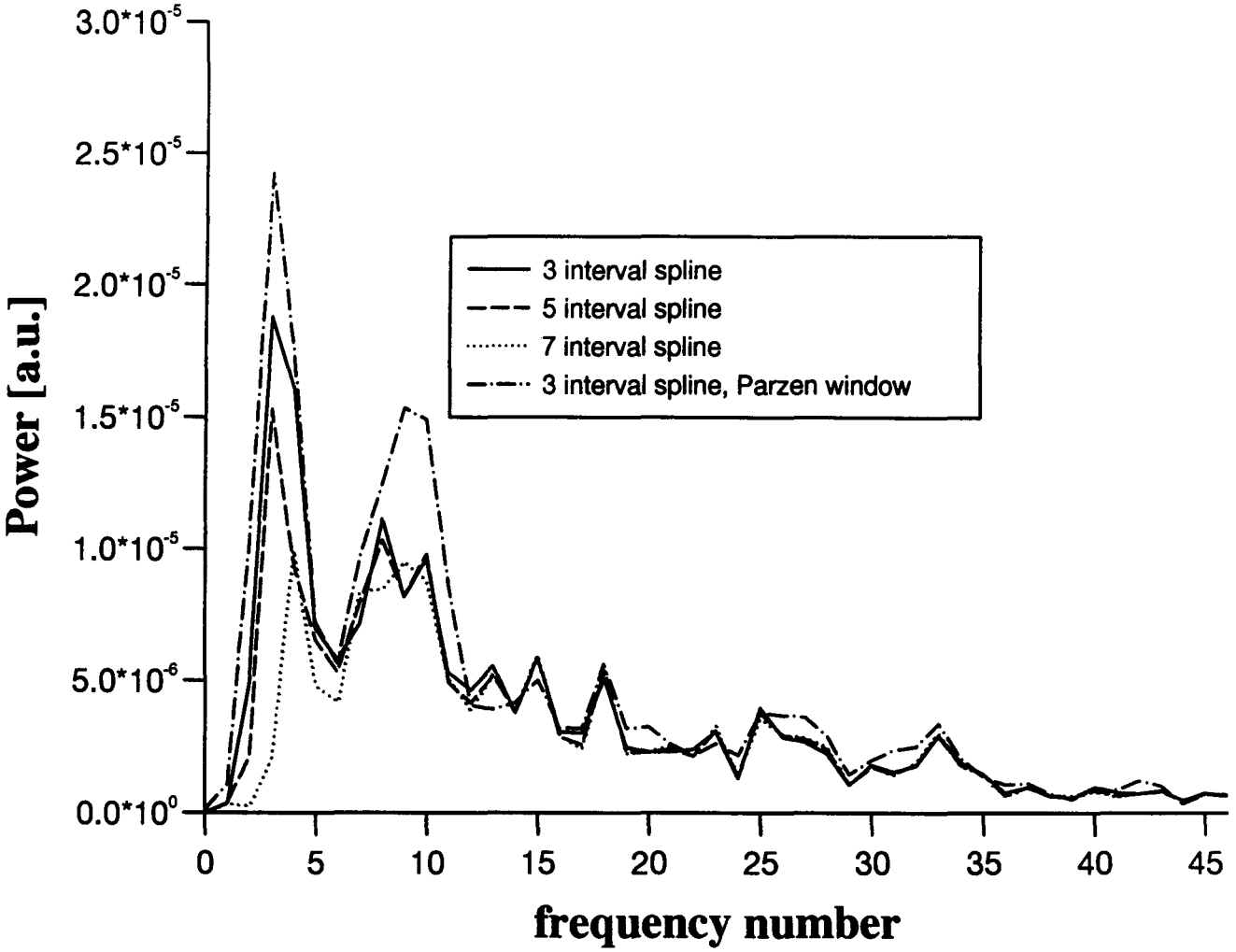

Figure A.3: *Spline fit subtraction with 3, 5 and 7 intervals.*

is fitted and therefore the low frequency peak is reduced to a 1000 times smaller peak. The peak has not completely disappeared, because the splines do not perfectly fit the global profiles. The 7 interval cubic splines do this better than the 3 interval cubic splines and therefore the low frequency peak is lower in the former case.

Because the there is no peak orders of magnitude higher than the rest, the disturbances of the neighbouring channels are lower and no windowing is needed. Nevertheless the efect of a Parzen window is also shown in Fig. A.3. In this case it increases the signal for lower frequencies. This may be an indication that the low frequency structures are situated more in the central part than in the edge part.

Another way of estimating the global profile is by smoothing the T_e profiles. In Fig. A.4 the results are shown for three different smoothing levels. Smoothing 11 means for example that the smoothed data point is obtained by averaging over the 11 nearest points. One would think that averaging over 11 points would filter out frequencies lower than $f_c = \frac{93}{11}$, but this is not

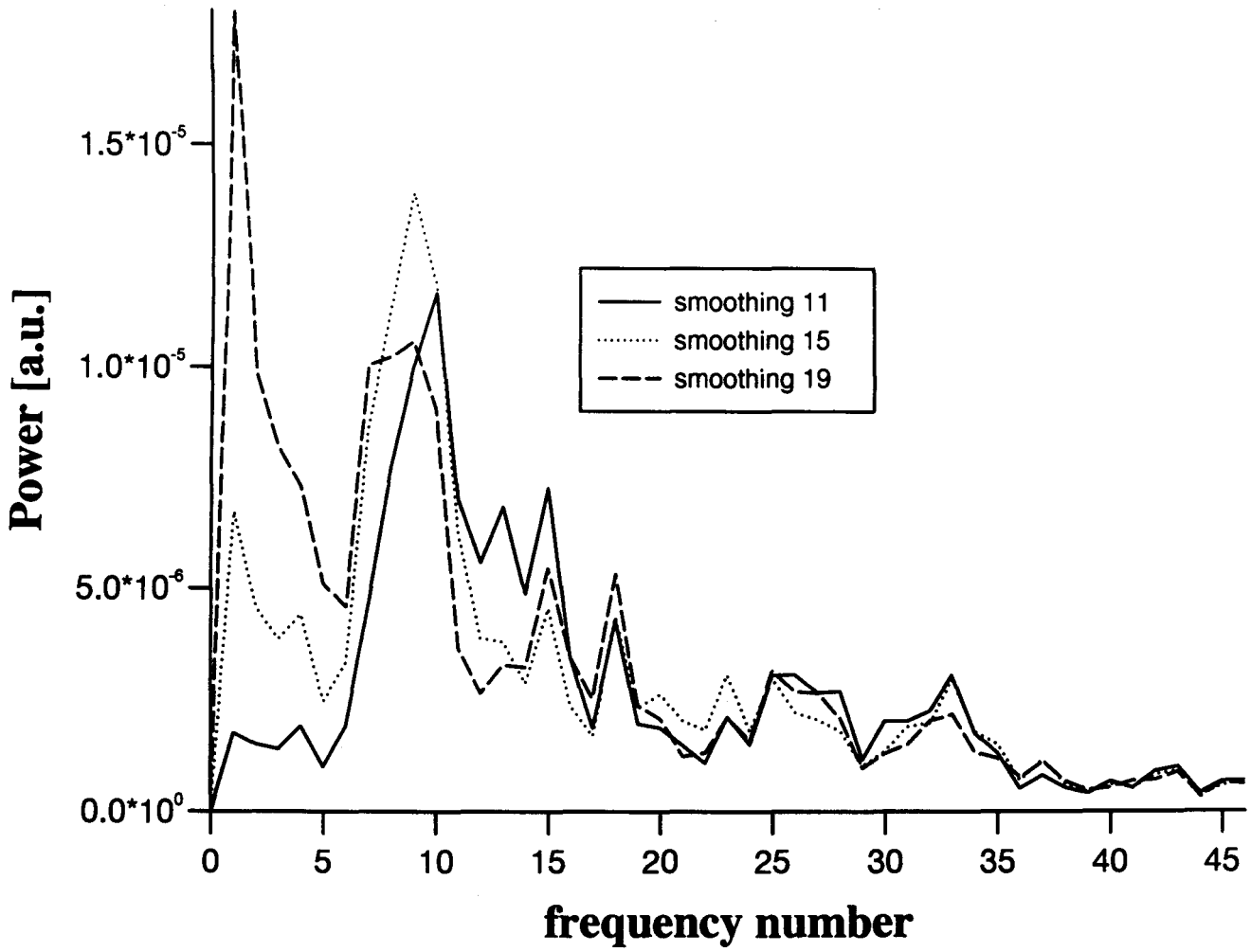

Figure A.4: *Power spectra of the profiles after subtraction of smoothed profiles.*

completely the case. Also lower frequencies appear in the spectrum and higher frequencies ar affected.
To test this further 1000 random profiles of 93 points were generated and smoothed. Th smoothed profiles were subtracted from the original random profiles and the power spectrun was calculated. The results are shown in Fig. A.5 for 6 smoothing levels. The cut off frequen cies (f_c) are also shown. The horizontal solid lines are the power spectra of the random profiles the dotted lines are the power spectra of the smoothed profiles and the dotted lines are th spectra of the random profiles from which the smooth profiles have been subtracted. Figure A. shows that smoothing is not a perfect filtering method, it affects the power spectra also for highe frequencies: Some oscillatory behaviour is visible. Another way to get rid of the high peak c Fig. A.2 is by dividing the profiles by their global profile, a sort of normalization. A quick chec showed that the power spectra look like spectra of Fig. A.3 except for a correction factor.
Of all possible ways of presenting the power spectra the first one, windowing of the data, seeme to me the best way.

Instead of averaging the power spectra of the individual profiles over the profiles of the dat set, it is also possible to put the profiles behind each other and calculate the power spectrum o

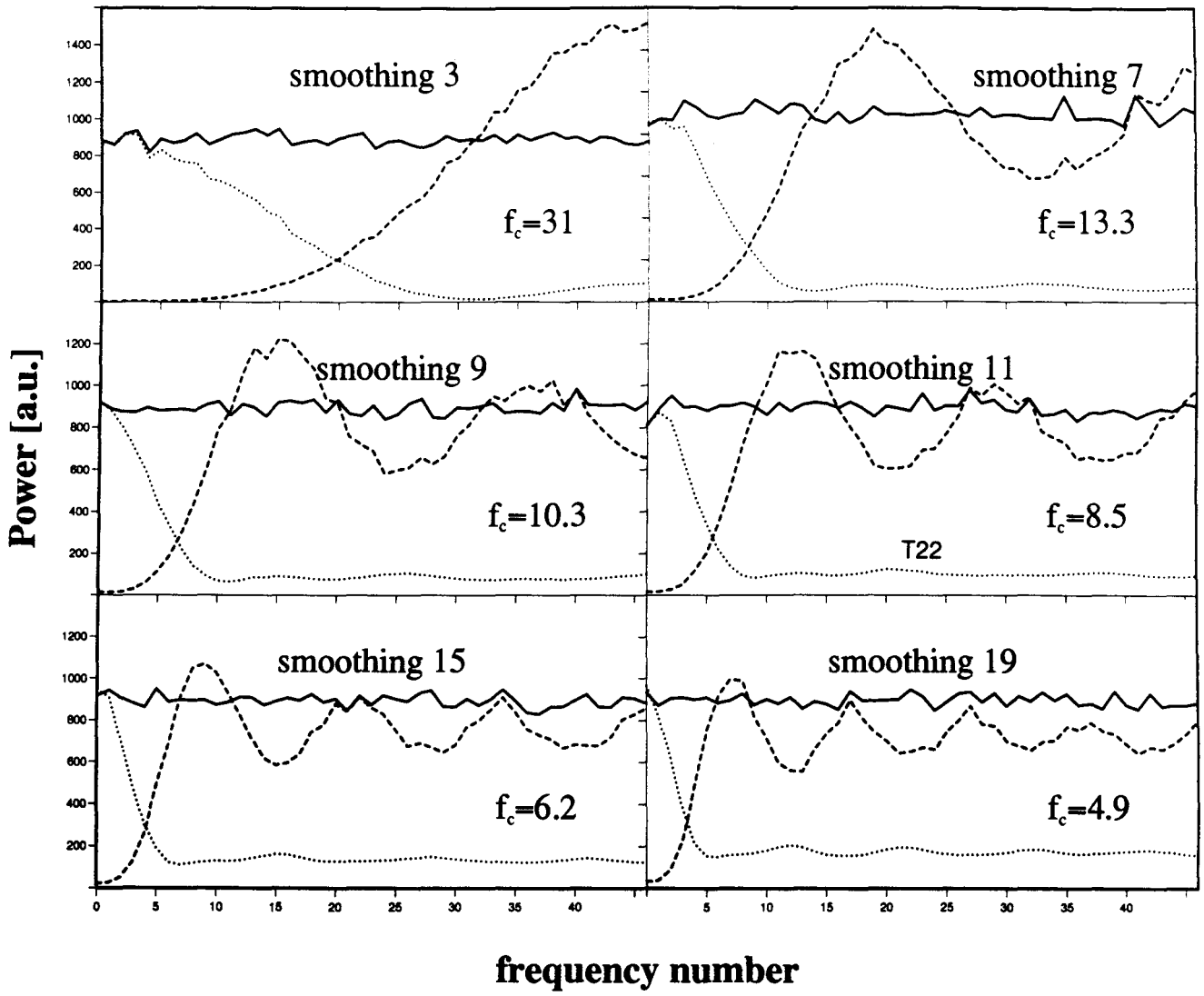

Figure A.5: *Test on effect of smoothing on power spectra.*

this bigger series of data. The power spectra shown in Fig. A.6 are calculated in this way for the ohmic data of set SU1 (Fig. A.6a) and ohmic data set of SU2 (Fig. A.6b). The slopes are about the same as in Fig. 6.1, the absolute values should be corrected according to Parseval's theorem if one wants to compare these values to the values of Fig. 6.1.

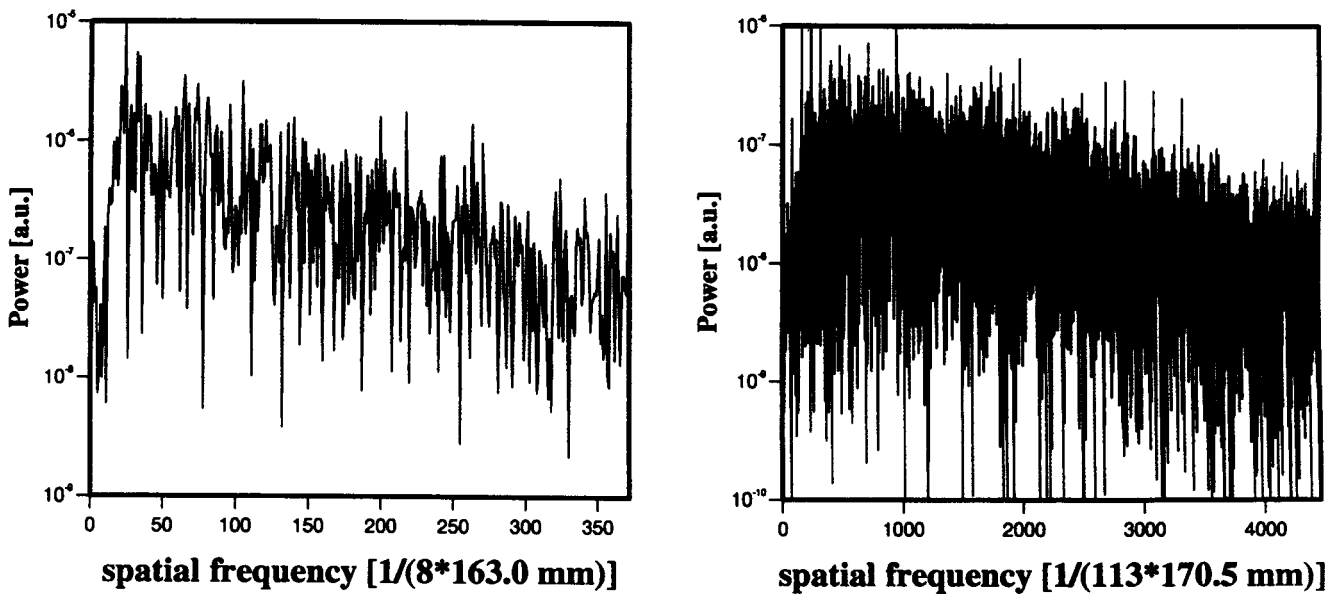

Figure A.6: *Power spectrum of a chain of T_e profiles, for the 8 SU1 ohmic discharges (left) and for the 79 SU2 ohmic discharges (right).*